Simulation of Atmospheric Variability[1]

SYUKURO MANABE AND DOUGLAS G. HAHN

Geophysical Fluid Dynamics Laboratory/NOAA, Princeton University, Princeton, NJ 08540

(Manuscript received 7 May 1981, in final form 3 August 1981)

ABSTRACT

A spectral atmospheric circulation model is time-integrated for approximately 18 years. The model has a global computational domain and realistic geography and topography. The model undergoes an annual cycle as daily values of seasonally varying insolation and sea surface temperature are prescribed without any interannual variation. It has a relatively low computational resolution with 15 spectral components retained in both zonal and meridional directions. Analysis of the results from the last 15 years of the time integration indicates that, in middle and high latitudes, the model approximately reproduces the observed geographical distribution of the variability (i.e., standard deviation) of daily, monthly and yearly mean surface pressure and temperature.

In the tropics, the model tends to underestimate the variability of surface pressure, particularly at longer time scales. This result suggests the importance of processes with long time scales such as ocean–atmosphere interaction, in maintaining the variability of the atmosphere in low latitudes.

It is shown that global mean values of standard deviation of daily, 5-daily, 10-daily, monthly, seasonal and annual mean surface pressure of the model atmosphere may be approximately fitted by a corresponding set of standard deviations of a red noise time series with a decay time scale of slightly longer than four days. However, it appears that the temporal variation of surface pressure also includes minor contributions from disturbances with much longer decay time scales.

In general, the model tends to underestimate the persistence (or decay time scale) of atmospheric disturbances. However, it reproduces some of the features of the observed geographical distribution of decay time scale of the surface pressure fluctuations in middle and high latitudes.

The observed standard deviation of annual, hemispheric mean surface air temperature also is compared with model results. Although a clearcut evaluation of model performance is somewhat hampered by observational uncertainty, it appears that the model's value amounts to a substantial fraction of the corresponding standard deviation derived from observational studies.

1. Introduction

Over the past two decades, the quality of atmospheric general circulation models (GCM's) has greatly improved. Some of the experimental results indicate that GCM's have successfully reproduced many of the basic characteristics in the time-mean state of the present climate. However, there have been very few studies which evaluate the temporal variability of a model atmosphere (e.g., Blackmon and Lau, 1980; Chervin, 1980), in particular, studies which investigate model variability at monthly, seasonal and interannual time scales. Since a large amount of computer time is required to time-integrate a GCM over an extended period of time (i.e., many years), the determination of the variability of a model atmosphere at these time scales has been difficult.

Two recent developments have resulted in an improved situation regarding direct evaluation of model variability. First of all, further technological improvements have yielded a substantial increase in computer speed; and second, the development of spectral GCMs with semi-implicit time integration schemes has resulted in the speed-up of the time-integration of the GCM's. Because of these developments, it has become feasible to perform a long-term integration of a spectral GCM with relatively low computational resolution.

One necessary condition for the effective evaluation of the variability of a simulated climate is the availability of observational data from which the corresponding variability of the actual atmosphere can be inferred. Such data has recently become available owing to the effort of Jenne (1975) and Oort (1982) who have compiled a massive amount of data from surface and upper air observations.

A successful simulation of climate variability by a mathematical model clearly is an important prerequisite for reliable studies on the predictability and the variability of climate using the model. When it is confirmed that a model succeeds in reproducing some of the essential characteristics of the ob-

[1] Preliminary results of this study are found in Hahn and Manabe (1979).

served variability of the atmosphere, one can use the model for the identification of dynamical and physical mechanisms responsible for climate variability. For example, by comparing results from two long term integrations of a model with and without a certain relevant process (e.g., ocean–atmosphere interaction, snow–albedo feedback), one can evaluate the influence of this process on the variability of climate. Such a variability study is the topic of a future investigation. In this study, variability of the simulated atmosphere is compared with that of the actual atmosphere. In addition, this study can yield information on the potential importance of some of the processes excluded from the model (e.g., ocean–atmosphere interaction) in controlling the variability of climate. (Note that, in the present model, the distribution of the seasonally varying sea surface temperature is prescribed and does not change from one year to the next.)

It is expected that this study also provides information essential for evaluation of results from a climate sensitivity study conducted with a general circulation model of the atmosphere. A sensitivity study compares two time-mean states which emerge from long-term integrations of a model with and without certain forcing. In order to evaluate the response of the model climate to the forcing, it is necessary to study the difference between the two time mean states of the model integrations in light of the natural variation (standard deviation) of its time-mean states. The variability of the time mean states of the model atmosphere is the subject of this study.

2. Model structure

A spectral model of the atmosphere used in this study is constructed by combining the framework of spectral dynamics as developed by Gordon and Stern (1974), with mathematical representations of the physical processes (e.g., moist and dry convection, radiation and ground hydrology, etc.) as previously developed at the Geophysical Fluid Dynamics Laboratory (GFDL) (Manabe, 1969; Holloway and Manabe, 1971). Here only a brief description of the model is presented; a more detailed description is found in Manabe *et al.* (1979).

The dynamical structure of the spectral atmospheric model is very similar to the spectral model developed by Bourke (1974). It predicts stream function and velocity potential for the horizontal components of the wind, temperature, moisture and surface pressure based on the equations of motion, the thermodynamical equation, the prognostic equation of water vapor, and the continuity equation of mass. The horizontal distributions of these variables are represented by a limited number of spherical harmonics. The resolution of the representation is determined by the degree of rhomboidal truncation of the spherical harmonics components. For this model, 15 zonal wavenumbers are retained. In the vertical direction, the distributions of the variables are specified at nine unequally spaced finite-difference levels which extend from the surface to ~25 km. The model has a global computational domain and realistic geography and topography.

Precipitation is predicted whenever the relative humidity exceeds 100% (Manabe *et al.*, 1965). The precipitation is identified as snowfall if the air temperature near the earth's surface falls below freezing; otherwise, rainfall is predicted (Manabe, 1969). At the continental surface, temperature is determined from the assumption that no heat is stored in the ground. Over the oceans, a seasonally and geographically varying sea surface temperature distribution derived from observations (Manabe *et al.*, 1979; U.S. Naval Oceanographic Office 1944, 1957, 1958, 1967a, 1967b, 1969) is prescribed. The annual cycle of sea surface temperature exactly repeats itself. Therefore, it has no interannual variation. The changes in soil moisture and snow cover over the continents are determined from the hydrology budget computations as derived by Manabe (1969). If snow cover is indicated, surface albedo is increased according to snow depth.

For the computation of the flux of solar radiation, the scheme of Lacis and Hansen (1974) is used after minor modification. The fluxes of terrestrial radiation are obtained using a scheme developed by Rodgers and Walshaw (1966) and modified by Stone and Manabe (1968). The seasonal, latitudinal distribution of insolation at the top of the model atmosphere is prescribed. Diurnal variation of insolation is not incorporated. The gaseous absorbers considered in the radiative transfer calculations are water vapor, carbon dioxide and ozone. The distribution of water vapor, which varies spatially and temporally, is obtained from the prognostic system of water vapor as mentioned above. Zonal mean distributions of ozone derived from observations are prescribed as a function of latitude, height, and season. On the other hand, it is assumed that the mixing ratio of carbon dioxide in air is constant everywhere; its prescribed concentration being 0.456×10^{-3} g g^{-1} of air. In addition, the radiative effects of cloud cover are taken into consideration by prescribing a latitude-pressure distribution of cloud cover which does not change with season.

The performance of the model in simulating the time mean state of the atmosphere and its seasonal variation was evaluated by Manabe *et al.* (1979). In particular, they investigated how the simulated climate is affected by the degree of spectral truncation of the model.

The model is time-integrated over 17.75 annual cycles starting from initial conditions obtained from

a 300-day integration of the model with fixed January distributions of insolation and sea surface temperature. From the 17.75 year record of this seasonal integration, the data from the last 15 years is analyzed and presented in this report. It is important to recognize that the model contains no interannual forcing resulting from fluctuations in sea surface temperature, ozone, cloud amounts or insolation, as the same values are prescribed for the corresponding data of each model year. However, the model climate may have interannual variability resulting from the physical processes related to snow cover and soil moisture, and internal dynamics of atmospheric circulation.

3. Observational data

In order to evaluate the performance of a GCM in simulating the variability of the atmosphere, it is desirable to have a global observational data set which has been collected over an extended period. As mentioned in the Introduction, the following two sets of observational data are used for model evaluation in this study.

The first set, compiled by Jenne (1975), contains distributions of daily sea level pressure for 73 years from 1899 to 1972. As discussed by Madden (1976), the quality of this data set is not uniform over this period mainly because the number and spacing of data reports varied greatly during this period and because of local changes in data analysis procedure. In order to reduce the distortion of climate variability attributable to such problems, only data from the last 15 years (1958–72) are used for model validation in this study. These data are compiled from digitization of the Northern Hemisphere daily weather maps on a 10° longitude × 10° latitude grid. Unfortunately, this data set extends only from 20 to 80°N and contains only the sea level pressure field.

The second data set used in this study is compiled by Oort and his collaborators at the Geophysical Fluid Dynamics Laboratory of NOAA using mainly the historical records of rawinsonde data for the 10-year period May 1963–April 1973. Unlike the previous data set, it extends over the entire globe and includes the statistics compiled for several atmospheric variables at atmospheric levels extending upward to 50 mb. This data tends to be most reliable in regions where the rawinsonde network is dense. On the other hand, it tends to be least reliable over some of the vast oceanic regions with little rawinsonde coverage, particularly south of 40°S, Oort (1978). For further discussion of this data set and the analysis procedures used in processing the data, see Stefanick (1981).

Additional observational reports available for use in validation of atmospheric GCM variability were compiled by van Loon (1967) and van Loon and Jenne (1974). They contain zonal mean standard deviation of daily values of sea level pressure and 500 mb geopotential height and standard deviation of monthly mean 500 and 100 mb geopotential height. These observed distributions have not been included in this report since they are not substantially different from those compiled from the previously mentioned data sets of Oort and Jenne.

4. Time-mean fields

To avoid a lengthy discussion, a comprehensive evaluation of the variability of all model variables is not attempted. Instead, emphasis is placed on evaluation of the model performance in simulating the variability of the key variables of pressure and temperature.

Before discussing variability of the model atmosphere, the time mean fields of sea level pressure and surface air temperature as simulated by the model are briefly described. Figs. 4.1 and 4.2 show the model's 15-year mean geographical distributions of sea level pressure for the Dec–Jan–Feb and Jun–Jul–Aug seasons. Corresponding observed distributions of sea level pressure, as compiled by Crutcher and Meserve (1970) and Taljaard *et al.* (1969), also are included in these figures for the sake of comparison. For both seasons, the distribution of observed sea level pressure is simulated by the model to a relatively high degree of accuracy despite the low computational resolution of the model. For example, in both seasons the intensities of the subtropical highs west of North America and North Africa are well simulated. However, they tend to be located too far north during the Jun–Jul–Aug season. Subtropical highs of the Southern Hemisphere west of Africa, South America, and Australia are well-positioned by the model in both seasons, although they tend to be slightly weak by ~1–5 mb.

During the Dec–Jan–Feb season, the model simulates an Icelandic low and a Siberian high of about the right intensity. However, the Aleutian low is too deep by ~10 mb and is placed too far north. The large-scale structure of the summer Asian low is simulated quite well by the model, although sea level pressures are ~5 mb too low over much of Asia and the western Pacific. In summer over other continents, namely, North America, South America and Africa, there exists a similar tendency for sea level pressures to be slightly lower than observed.

In both seasons, the model is unable to accurately simulate the low-pressure belt along the Antarctic coast. However, these results for the region north of the Antarctic coast are more realistic than many of the previous simulations using finite-difference models (e.g., Holloway and Manabe, 1971).

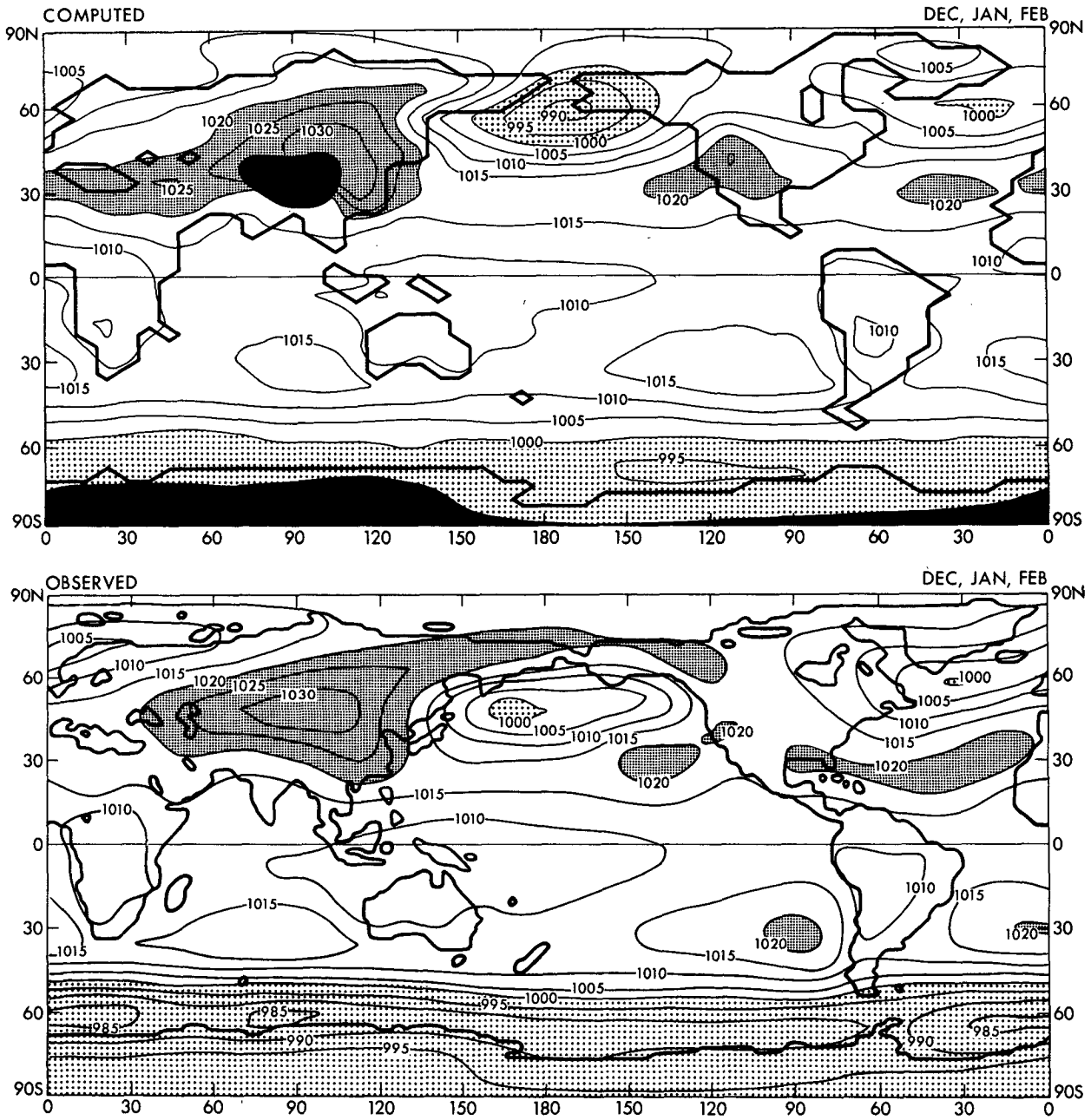

FIG. 4.1. Geographical distributions of sea level pressure (mb) for Dec–Jan–Feb season. Top: the 15-year mean distribution of the model. Bottom: the observed distribution from the data sets of Crutcher and Meserve (1970) and Taljaard *et al.* (1969).

Figs. 4.3 and 4.4 include geographical distributions of seasonal mean surface air temperature which have been constructed in a manner similar to that of the preceding two figures. Computed "surface air temperature" is the temperature at the lowest finite-difference level of the model, which is located at ~70 m above the earth's surface and is somewhat higher than the level where surface air temperature is usually observed. This difference introduces a small bias which tends to make computed surface air temperatures appear lower than observed. Since sea surface temperatures of the model are set equal to observed climatological means, it is not surprising that one finds reasonably good agreement between the computed and observed distributions of surface air temperature over oceanic regions. Over continental regions in summer, surface air temperatures of the model tend to be higher than observed for an unidentified reason. Otherwise, the model reproduces the basic characteristics of the geo-

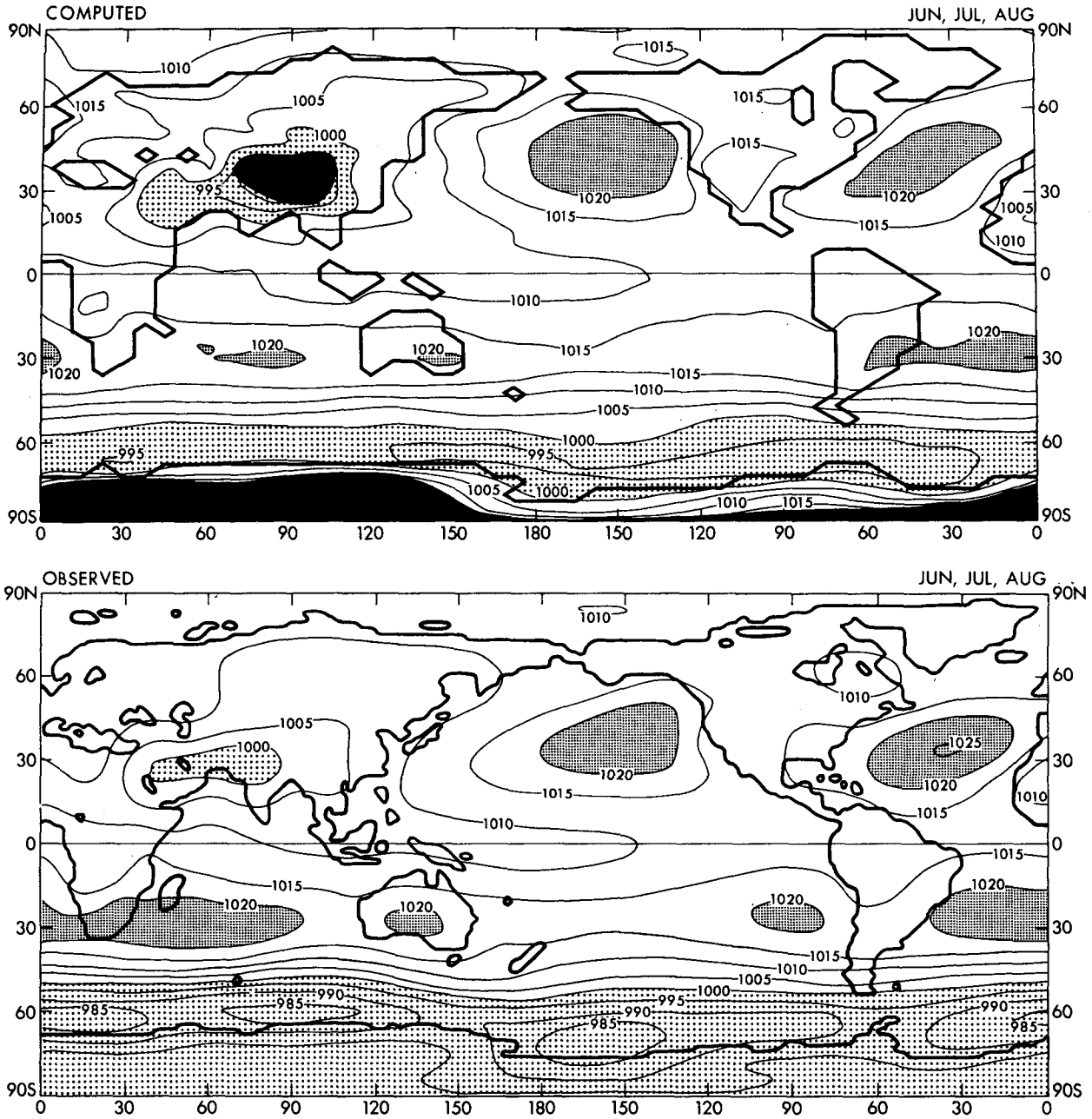

FIG. 4.2. As in Fig. 4.1 except for the Jun–Jul–Aug season.

graphical and seasonal variation of observed surface air temperature. For example, the model reproduces areas of minimum temperature in the northern portion of the Eurasian and North American continents in the Dec–Jan–Feb season.

5. Variability of pressure

a. Geographical distributions

In order to examine variability of the model atmosphere at several time scales, standard deviations of daily data, 5-day means, 10-day means, monthly means, seasonal means, and annual means are computed using the 15-year model data set. Here, the standard deviation σ_T of the field ϕ averaged over period T (i.e., $\bar{\sigma}^T$) is defined by

$$\sigma_T = \left[\frac{1}{N-1}\sum_{n=1}^{N}\left(\bar{\phi}_n{}^T - \frac{1}{N}\sum_{n=1}^{N}\bar{\phi}_n{}^T\right)^2\right]^{1/2}, \quad (1)$$

where N is the number of model years (15) for which the present analysis is conducted. From this

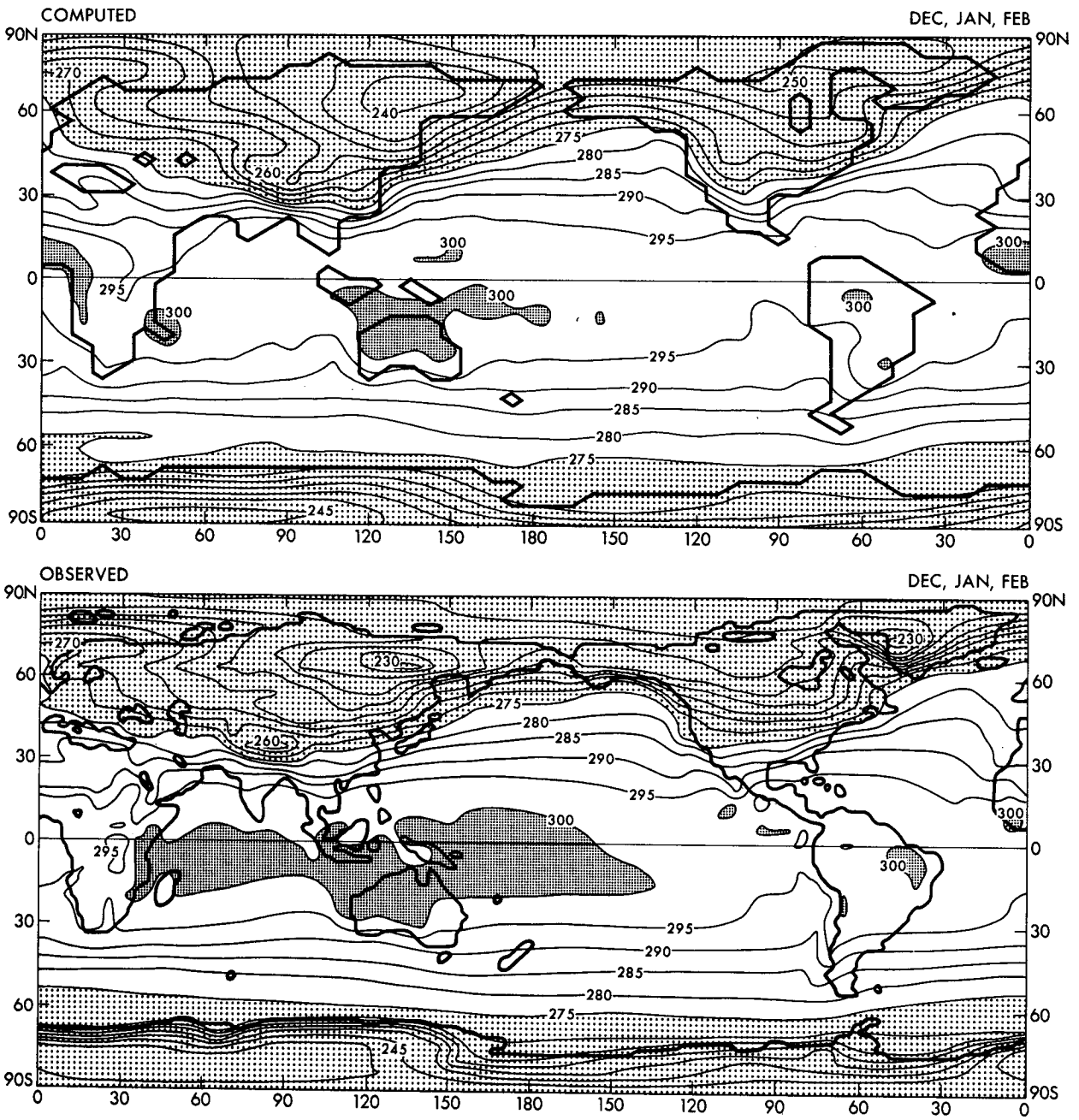

FIG. 4.3. Geographical distribution of surface air temperature (K) for the Dec–Jan–Feb season. Top: the 15 year mean distribution from the model. Bottom: the observed distribution from the data sets of Crutcher and Meserve (1970) and Taljaard *et al.* (1969).

equation, it is clear that fluctuations of the time means, which are considered for the computation of standard deviation, do not include a contribution from the mean annual cycle. For computational convenience, variance of daily fluctuation (σ^2) averaged over the period of one month is not computed from Eq. (1). Instead, it is approximated as the sum of 1) the variance calculated using daily departures from each monthly mean and 2) the variance of the 15 monthly means as determined from Eq. (1). See Chervin (1980) for further discussion of this approximation.

Fig. 5.1 compares the standard deviation of daily 1000 mb geopotential height of the model for the Dec–Jan–Feb season with the corresponding standard deviation deduced from the observational data of Oort. For both computed and observed distributions, the seasonal mean daily variances, from which standard deviations are obtained, are arithmetic averages of three monthly mean daily

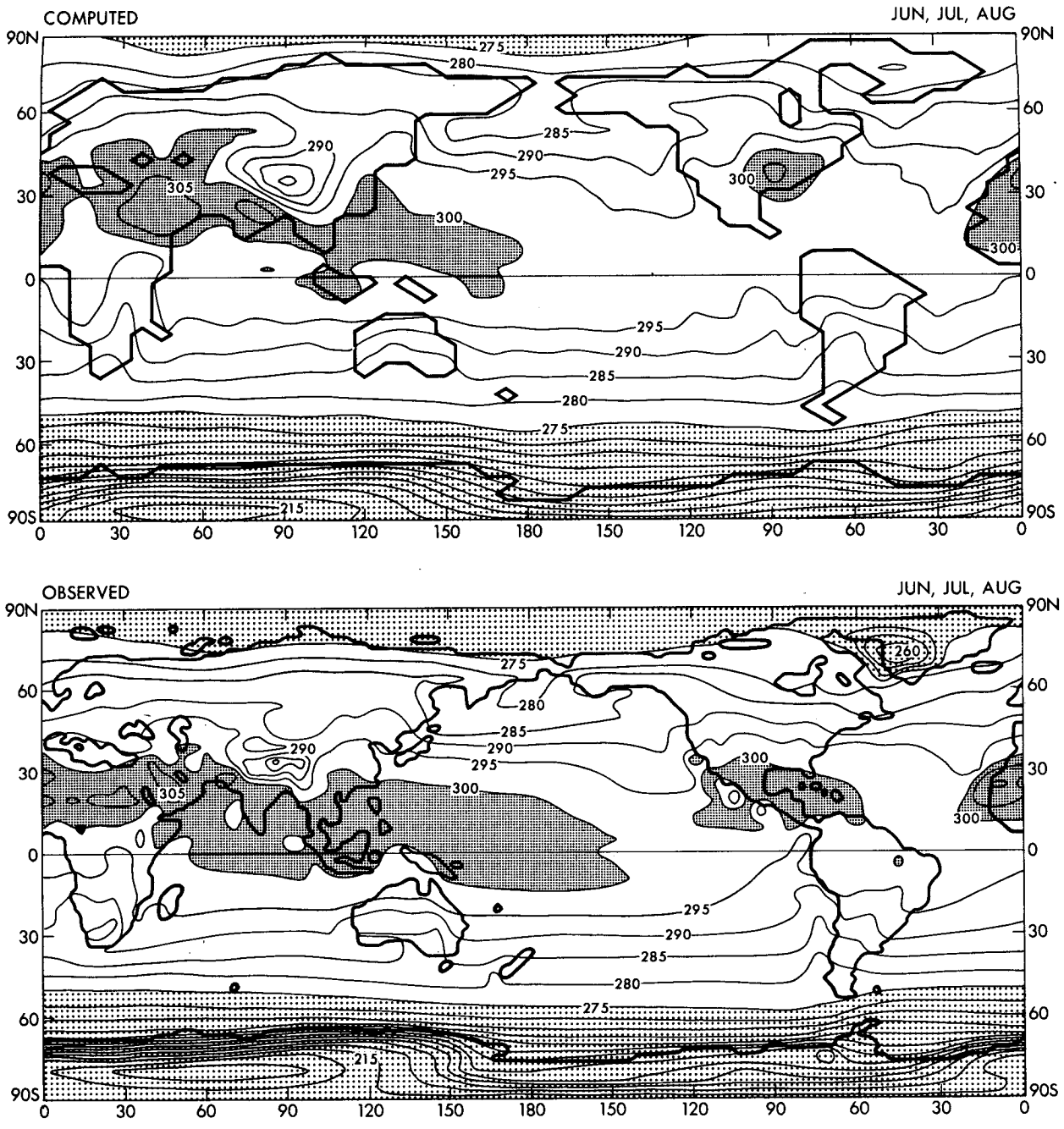

FIG. 4.4. As in Fig. 4.3 except for the Jun–Jul–Aug season.

variances. This comparison indicates that the model reproduces most of the features of the observed distribution of the standard deviation of daily 1000 mb geopotential height. For example, in the Dec–Jan–Feb season, the model simulates maxima near the vicinity of the Icelandic and Aleutian lows and along the Arctic coast of central Eurasia though these maxima tend to be situated too far north. Meridional belts of relatively small values observed in east central North America, along the east coast of Asia, and along the west coasts of North America, South America, Australia and Africa also are indicated in the model distribution.

For the Jun–Jul–Aug season, results in Fig. 5.2 also show that the model is successful in simulating the daily variability of 1000 mb geopotential height. For example, the model produces maxima of standard deviation in the vicinity of Iceland and the Aleutians. Unfortunately, the model maintains an east Asian maximum which is not evident in the

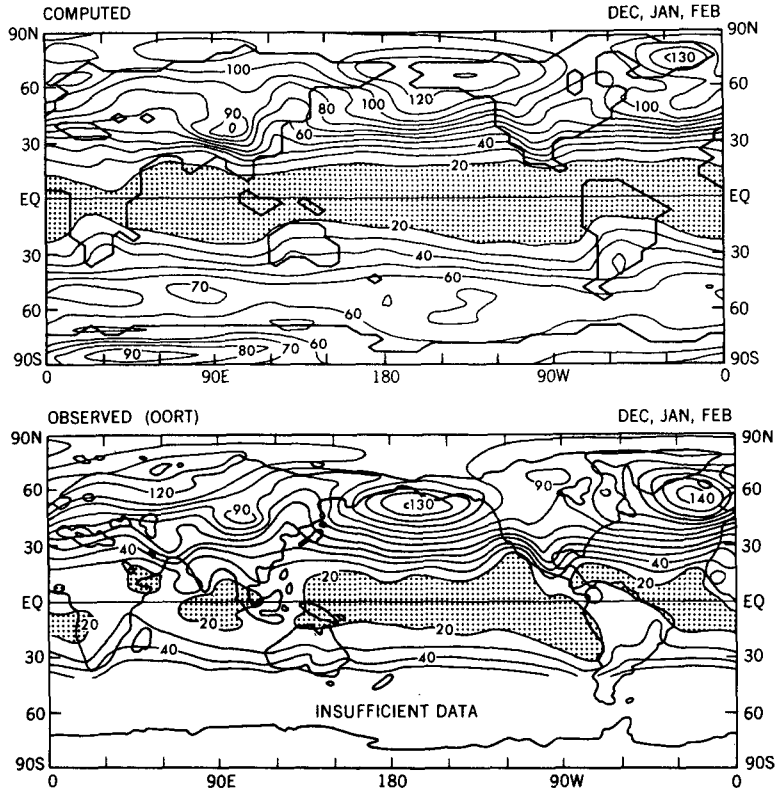

FIG. 5.1. Standard deviation of daily geopotential height (m) at the 1000 mb surface for the Dec–Jan–Feb season. Top: simulated. Bottom: observed, Oort.

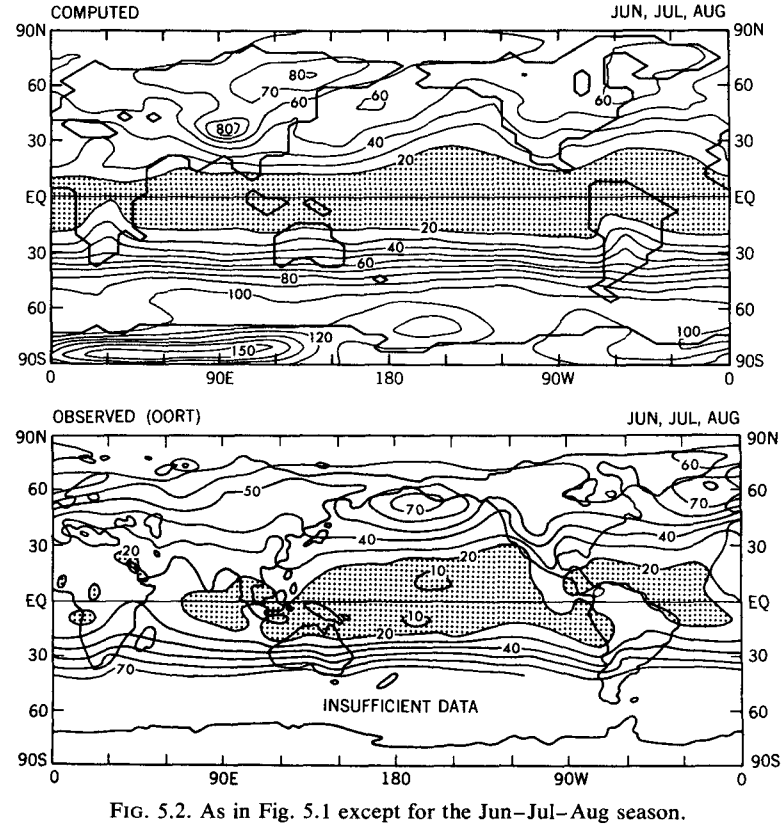

FIG. 5.2. As in Fig. 5.1 except for the Jun–Jul–Aug season.

observed distribution. Meridional belts of relatively small values are indicated in the simulated distribution along the west coasts of North America and Africa in qualitative agreement with the observed characteristics. In general, the gross features of the simulated and observed variability distributions of the Dec–Jan–Feb season qualitatively resemble those of the Jun–Jul–Aug season. The main difference is that the magnitudes of regional maxima of the winter season tend to be almost twice as large as those of the summer season.

Some of the unrealistic features of the simulation identified above appear to be related to the features of the sea level pressure distribution of the model. For example, standard deviation of daily 1000 mb geopotential height during the Jun–Jul–Aug season is generally larger in the model than observed over eastern Siberia and the western Pacific. Similarly, in the Dec–Jan–Feb season, the Aleutian region of large variability is more extensive in the model than observed. In both cases, sea level pressure is shown to be lower than observed as indicated by Figs. 4.1 and 4.2, suggesting that these model failures are related to one another. In addition, near the Aleutians and Iceland in the Jun–Jul–Aug season, daily variability of the model is shown to be less than observed. In this case, sea level pressure was previously shown to be higher than observed as the oceanic subtropical highs of the model extend too far poleward over the North Pacific and the North Atlantic. These examples suggest that in the model atmosphere, the activity of atmospheric disturbances is more intense than observed in regions where sea level pressure is lower than observed, and vice versa.

Geographical distributions of standard deviation of monthly mean 1000 mb geopotential height of the model are compared with observed distributions in Fig. 5.3 for the Dec–Jan–Feb season and in Fig. 5.4 for the Jun–Jul–Aug season. For both observed and computed distributions in both seasons, the geographical distribution of standard deviation of monthly mean 1000 mb geopotential height resembles the standard deviation of daily 1000 mb geopotential height shown in Figs. 5.1 and 5.2. As a result, Figs. 5.3 and 5.4 indicate that the successes and failures of the model in simulating the observed monthly variability patterns are similar in nature to those previously discussed regarding daily variability. For example, in the Dec–Jan–Feb season, centers of maximum standard deviation of monthly mean 1000 mb geopotential height are located near the Aleutians and Iceland with a tendency for small values to be located along the east coast of Asia and over continental North America. As previously

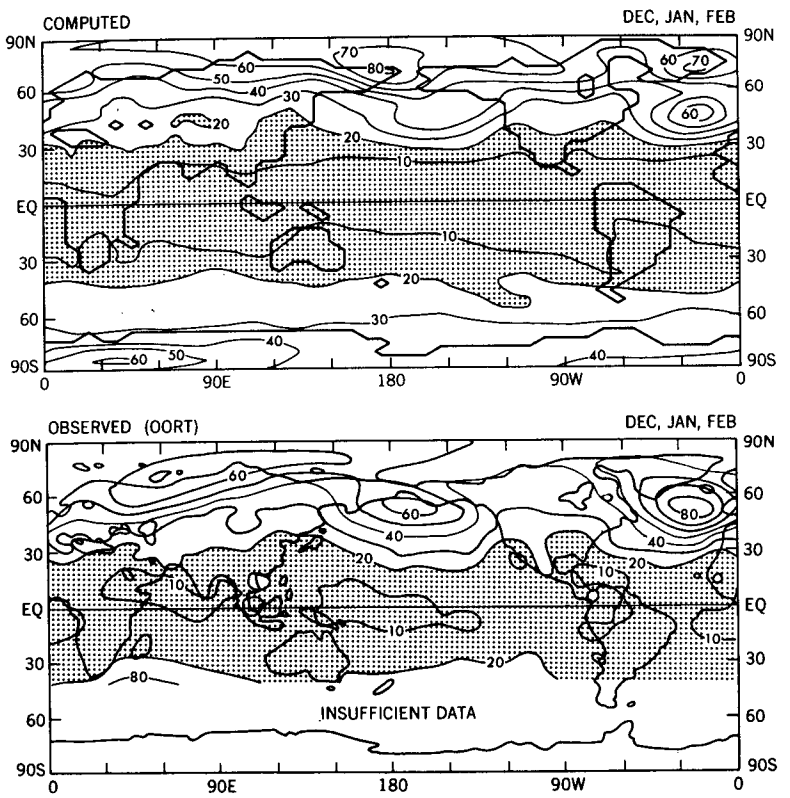

FIG. 5.3. Standard deviation of monthly mean 1000 mb geopotential height (m) for the Dec–Jan–Feb season. Top: simulated. Bottom: observed, Oort.

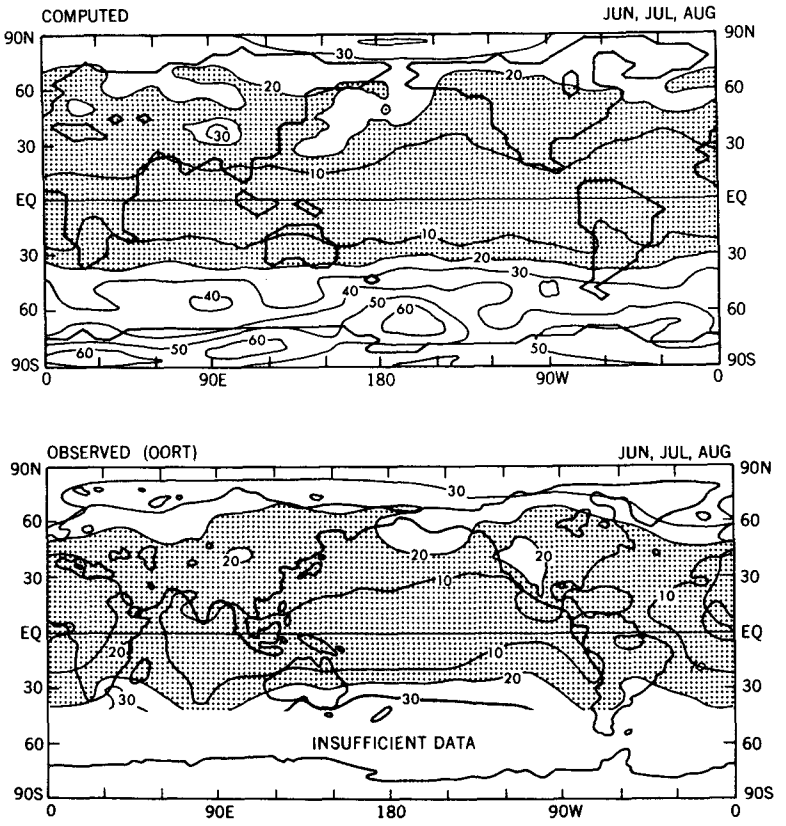

FIG. 5.4. As in Fig. 5.3 except for the Jun–Jul–Aug season.

stated with respect to daily variability, the model tends to overestimate monthly variability in regions where computed sea level pressures are lower than observed, i.e., over eastern Siberia and the western Pacific in the Jun–Jul–Aug season and near the Bering Strait in the Dec–Jan–Feb season.

In the tropics, standard deviation of monthly mean 1000 mb geopotential height is somewhat lower than observed, particularly in the Dec–Jan–Feb season as indicated by Fig. 5.3. In this season, the model fails to reproduce the relatively large variability in the tropical eastern Pacific.

Fig. 5.5 compares the standard deviation of annual mean 1000 mb geopotential height of the model with that of the actual atmosphere. The observed distribution of Fig. 5.5 is calculated using the annual means in the record of Jenne. According to this figure, the annual variability is relatively large near the Aleutians and Iceland in agreement with the observations. Qualitatively similar features are evident in the distributions of daily and monthly variability described earlier. In general the geographical distribution of standard deviation of annual mean 1000 mb geopotential height resembles the distributions of standard deviation of daily and monthly mean 1000 mb geopotential height in Figs. 5.1, 5.2, 5.3 and 5.4.

b. Zonal means

Fig. 5.6 contains latitudinal distributions of zonal mean standard deviation[2] of daily and monthly mean 1000 mb geopotential height for the Dec–Jan–Feb season of the model and in the actual atmosphere (Oort, Jenne). Fig. 5.7 contains similar distributions for the Jun–Jul–Aug season. These figures indicate that the model simulates the latitudinal and seasonal variation of zonally averaged standard deviation of daily and monthly mean 1000 mb geopotential height to a relatively high degree. Moreover, they also reveal that the observed variability obtained by Oort is in general agreement with the variability from the observational data of Jenne.

In high latitudes of the Northern Hemisphere in the Dec–Jan–Feb season, the latitude of maximum daily and monthly variability of the model is located poleward of the observed maxima as obtained by Oort and Jenne. This poleward shift of both daily and monthly variability in the Dec–Jan–Feb season is previously noted in the discussion of geographical distributions in Figs. 5.1 and 5.3.

[2] Hereafter zonal mean standard deviation is computed by averaging standard deviation (not variance) at all grid points along a latitude circle.

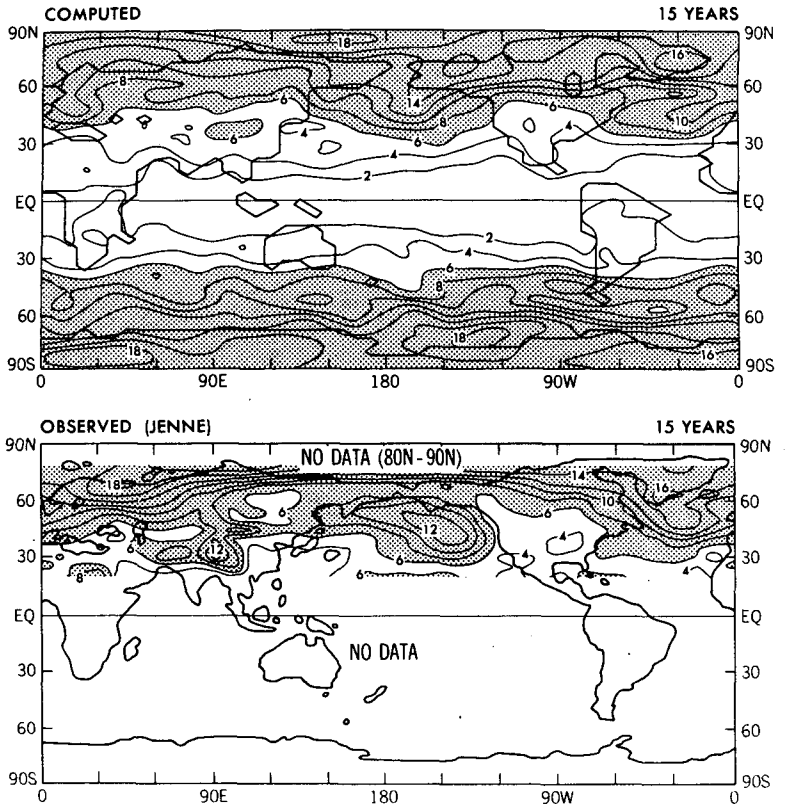

FIG. 5.5. Standard deviation of annual mean geopotential height (m) at the 1000 mb surface. Top: simulated. Bottom: observed, Jenne.

In the Jun–Jul–Aug season from approximately 15 to 50°N, standard deviations of both daily and monthly mean 1000 mb geopotential height of the model tend to be larger than observed. At these latitudes, it was shown that daily and monthly variability of the model have a tendency to be larger than observed over eastern Asia and the western Pacific.

In the tropics, Figs. 5.6 and 5.7 indicate that both simulated and observed estimates of atmospheric variability are small relative to the variability at other latitudes. However, the model tends to systematically underestimate the observed variability in the tropics. Also, the fractional difference between computed and observed variability is largest in this region. For example, in the Dec–Jan–Feb season, the model maintains ~70% of the daily and ~45% of the monthly variability as measured by the zonal mean standard deviations of geopotential height at the 1000 mb level at the equator. This suggests that the model's ability to simulate the variability of the actual tropical atmosphere decreases as the averaging period is increased from one day to one month.

The latitudinal distribution of zonally averaged standard deviation of annual mean geopotential height at the 1000 mb surface of the model is compared with an observed distribution in Fig. 5.8. At the latitudes where observational data of Jenne are available, the model variability of annual means matches well with that of the observations. This agreement is of particular interest in view of the fact that the process of ocean–atmosphere interaction, which can generate long-term fluctuations of climate, is not incorporated in the present model.

In Fig. 5.9, a latitude–pressure distribution of zonal mean standard deviation of daily geopotential height in the model atmosphere for the Dec–Jan–Feb season is compared with the observed distribution obtained from the data of Oort. This figure indicates that daily variability sharply increases with increasing latitude near 30°N and 30°S at all tropospheric levels of the model, in qualitative agreement with observations. However, the model's variability in the tropics is significantly smaller than observed, particularly in the upper troposphere and stratosphere.

At sea level, it was previously shown that the model simulates the latitudinal distribution of daily variability to a relatively high degree of accuracy.

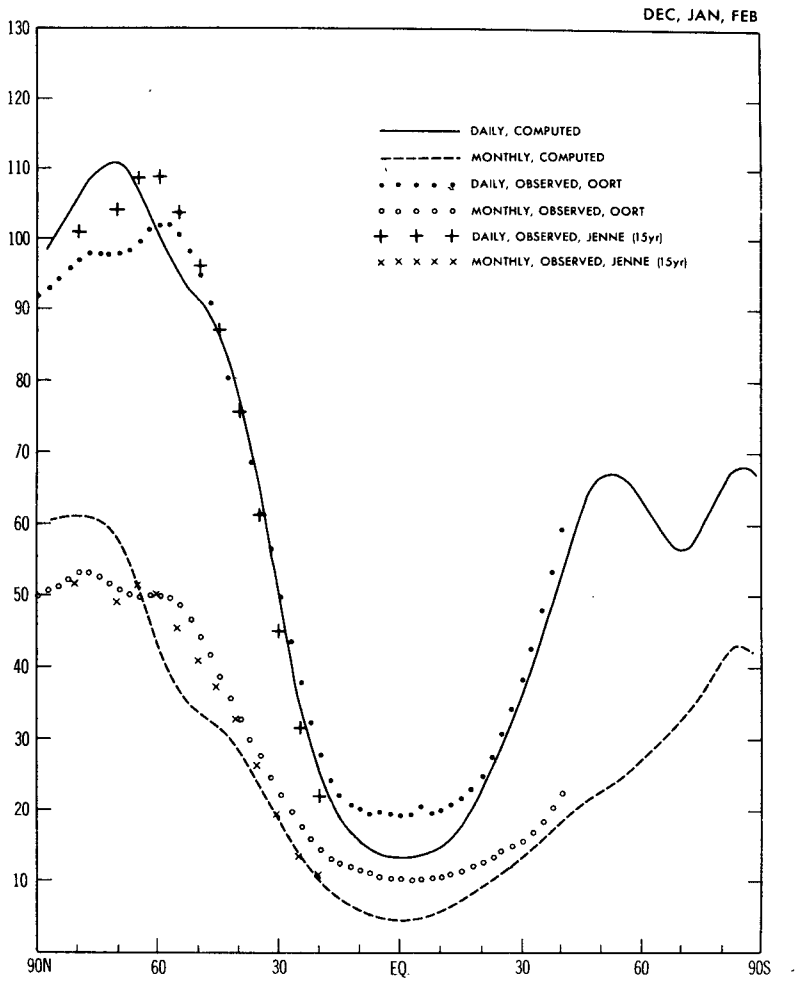

FIG. 5.6. Zonal means of standard deviation of daily and monthly mean 1000 mb geopotential height (m) for the Dec–Jan–Feb season. Observed distributions are from Oort and Jenne.

However, in the middle and upper troposphere, model values are systematically smaller than observed values, with the discrepancy increasing with increasing height. In addition, local maxima are observed near the tropopause at 60°N. Clearly, model profiles do not include this feature of the Northern Hemisphere. However, its characteristics are duplicated to some extent near the tropopause of the Southern Hemisphere.

The latitude–pressure profile of zonally averaged standard deviation of monthly mean geopotential height of the model is shown in Fig. 5.10 for the Dec–Jan–Feb season. The observed distribution (Oort) is also included in this figure for comparison. For both computed and observed distributions, the characteristics of monthly variability shown in Fig. 5.10 are similar to the characteristics of daily variability illustrated in Fig. 5.9, though the magnitude of standard deviation is reduced. Consequently, the assessment of the simulated monthly variability profiles as compared with the observed profiles is very similar to the corresponding evaluation of daily variability.

In tropical regions, the simulation of observed variability of monthly mean geopotential height is somewhat worse than the simulation of daily variability, particularly in the upper troposphere and lower stratosphere. For example, the daily variability of the model atmosphere is about one-half the observed value in the upper levels of the tropics as Fig. 5.9 indicates, whereas the variability of monthly means amounts to only about one third the observed value as revealed by Fig. 5.10.

In summary, the model successfully simulates the gross characteristics of the profile of zonal mean variability of daily and monthly mean geopotential

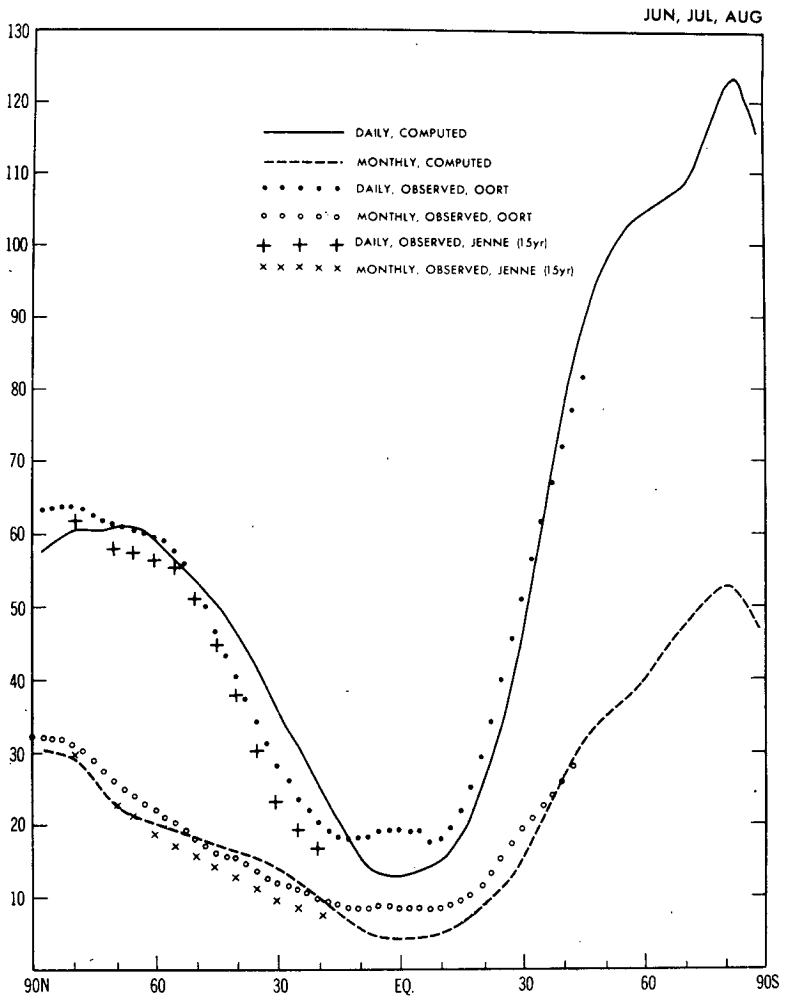

FIG. 5.7. As in Fig. 5.6 except for the Jun–Jul–Aug season.

height. The quality of the model simulation tends to decrease with increasing height and decreasing latitude.

c. *Global and hemispheric averages*

Leith (1973) and Madden (1976) pointed out that the daily fluctuation of sea level pressure in the actual atmosphere may be fitted approximately by a simple stochastic model of a first-order Markov process. If similar characterization applies to the daily fluctuation of pressure in the model atmosphere and the decay time scale of the fluctuation does not vary too much from one place to another, it is reasonable that the distribution of daily pressure variability qualitatively resembles the corresponding distributions for the monthly and yearly mean pressure as shown in the preceding subsections. This

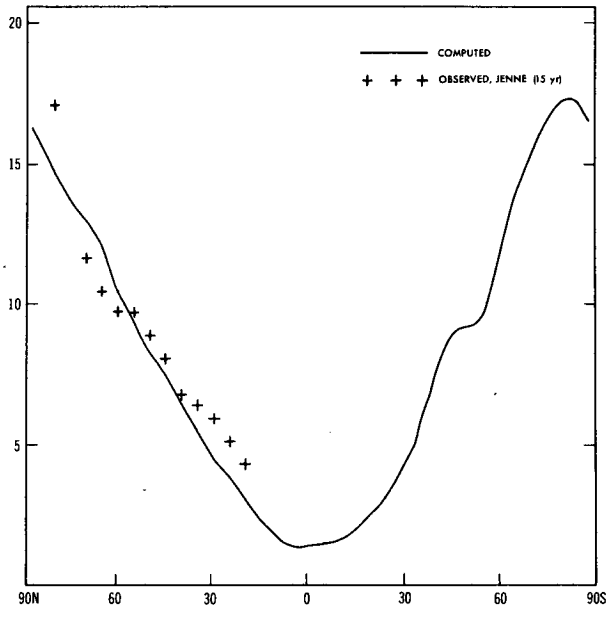

FIG. 5.8. Zonal means of standard deviation of annual mean geopotential height (m) at the 1000 mb surface for the model and observed (Jenne).

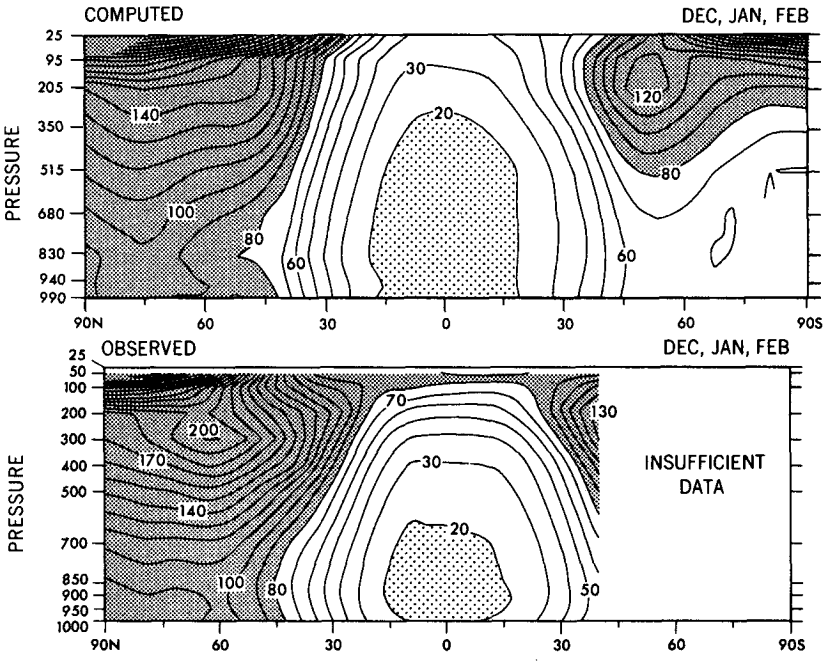

FIG. 5.9. Latitude–pressure distributions of zonal mean standard deviation of daily geopotential height (m) for the Dec–Jan–Feb season. Top: simulated. Bottom: observed, Oort.

section evaluates how well the daily 1000 mb geopotential height data resemble a red noise time series.

According to Leith (1973), the standard deviation of a red noise time series averaged over the period T (i.e., σ_T) is given by

$$\left(\frac{\sigma_T}{\sigma}\right)^2 = \frac{\tau_0}{T}\left\{1 - \frac{\tau_0}{2T}\left[1 - \exp\left(-\frac{2T}{\tau_0}\right)\right]\right\}, \quad (2)$$

where σ indicates the standard deviation of daily data, and τ_0 is a single correlation decay time scale defined by

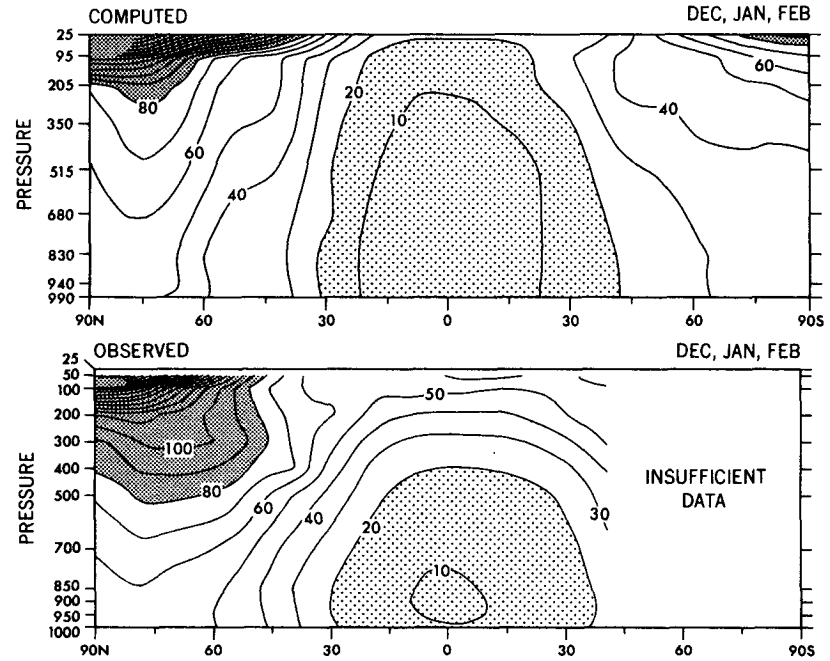

FIG. 5.10. Latitude–pressure distributions of zonal mean standard deviation of monthly mean geopotential height (m) for the Dec–Jan–Feb season. Top: simulated. Bottom: observed, Oort.

$$\tau_0 \equiv \int_{-\infty}^{\infty} R(\tau)d\tau, \qquad (3)$$

where $R(\tau)$ is the correlation at lag time τ. For a red noise time series, it is given by

$$R(\tau) = \exp\left(-\frac{2|\tau|}{\tau_0}\right). \qquad (4)$$

Here an attempt is made to determine how well Eq. (2) approximates the dependence of the standard deviation of time-mean geopotential height upon the averaging period.

For this purpose, the global average standard deviation of time-mean geopotential height of the 1000 mb level (i.e., $\tilde{\sigma}_T{}^G$) is computed for various lengths of the time-averaging period (i.e., T = 5, 10 days, month, season and year). These global averages are further normalized by the global average standard deviation of daily geopotential height (i.e., $\tilde{\sigma}^G$) and are plotted in Fig. 5.11. In addition, red noise curves, which show the relationship between (σ_T/σ) and T for a red noise time series, are determined for various values of τ_0 from Eq. (2) and are drawn for the sake of comparison. This figure shows that the dependence of normalized global mean-average standard deviation of time-mean geopotential height on the averaging period T can be represented approximately by a red noise curve with a decay time scale of approximately five days.

Upon further examination of Fig. 5.11, one notes,

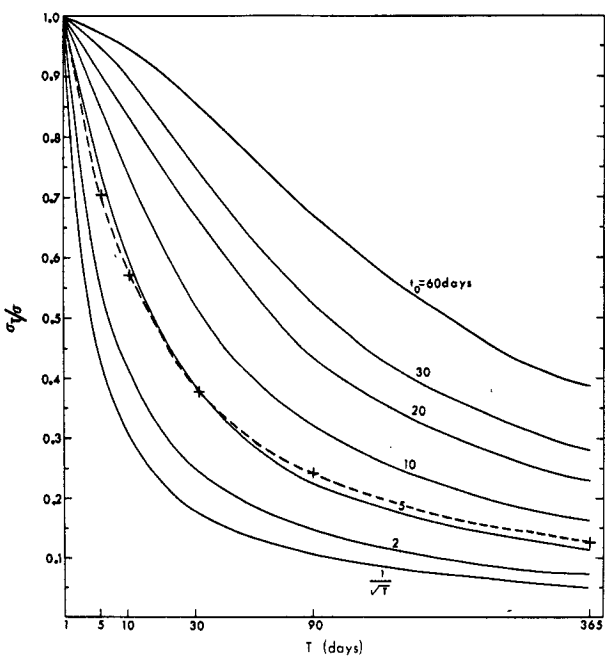

FIG. 5.11. Normalized global mean standard deviations of time averaged geopotential height at 1000 mb level of the model atmosphere are plotted by Crosses. (Ordinate: $\tilde{\sigma}_T^G/\tilde{\sigma}^G$. Abscissa: time-averaging period T). All standard deviations are computed from variances averaged over the annual cycle. The red noise curves for various decay time scales are added for comparison.

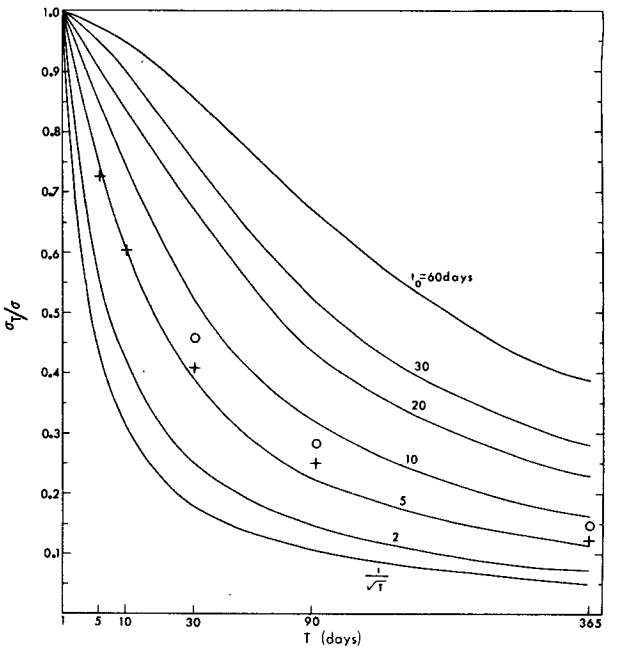

FIG. 5.12. Normalized area mean standard deviations of time averaged 1000 mb geopotential heights $\tilde{\sigma}_T{}^N/\tilde{\sigma}^N$ are plotted against the averaging period T. All standard deviations are computed from variances averaged over the annual cycle. [Here, $(\bar{\ })^N$ denotes the averaging operator over the area of the earth 20–90°N.] Crosses: simulated. Circles: observed, Jenne. The red-noise curves for various decay time scales are also added for comparison.

however, significant difference between $(\tilde{\sigma}_T{}^G/\tilde{\sigma}^G)$ plots of time-mean geopotential height and the red noise model curve of τ_0 = 5 days. For example, the plot for the averaging period of five days is on the red noise line of 4.4 days, whereas the plots for the averaging period of 10, 30, 90 and 365 days are on the red-noise line for which τ_0 is equal to 4.5, 5.1, 5.5, and 5.4 days, respectively. In short, the effective τ_0 values increase with increasing averaging period T. These results indicate that the records of temporal fluctuation of 1000 mb geopotential height in the model atmosphere cannot be regarded simply as the time series of red noise with a decay time scale of 4 ~ 5 days. Instead, they appear to contain the disturbances with longer decay time scales. [See the companion paper by Lau (1981) for the description of the structure of such disturbances which appear in the model atmosphere.]

To compare the normalized standard deviations of time-mean 1000 mb geopotential heights in the model atmosphere discussed above with those of the actual atmosphere, Fig. 5.12 is constructed. This figure contains the plots of $(\tilde{\sigma}_T{}^N/\tilde{\sigma}^N)$ versus T for both the model and the actual atmosphere. Here $(\bar{\ })^N$ indicates the area average over the latitudinal belt 20 to 90°N. This choice of region is dictated by the areal coverage of the observational data of Jenne (1975) used for this analysis. Red-noise curves are also drawn in this figure for reference. For the actual

atmosphere, normalized standard deviations of monthly, seasonal and annual mean 1000 mb geopotential height are positioned on red noise curves with τ_0 of 7.4, 7.7 and 8.3 days, respectively. For the model atmosphere, they are located on the red-noise curves with τ_0 of 5.6, 6.1 and 5.5 days, respectively. These results indicate that the decay time scale (τ_0) of disturbances in the actual atmosphere is significantly longer than the corresponding time scale in the model atmosphere. This discrepancy manifests itself in the decay time-scale analysis of the pressure field of the model atmosphere described in the following subsection.

d. Persistence

In this subsection, the distribution of the decay time scale is examined and is compared with the observed distribution. Assuming the time series can be fitted by a first-order Markov model, the decay time scale τ_0 defined by Eq. (3) is computed using the following approximation:

$$\tau_0 \simeq (\sigma_T/\sigma)^2 T. \tag{5}$$

This equation holds when $T \gg \tau_0$ [see Eq. (2)]. For the present analysis, T is chosen to be 30 days.

The geographical distribution of τ_0 computed

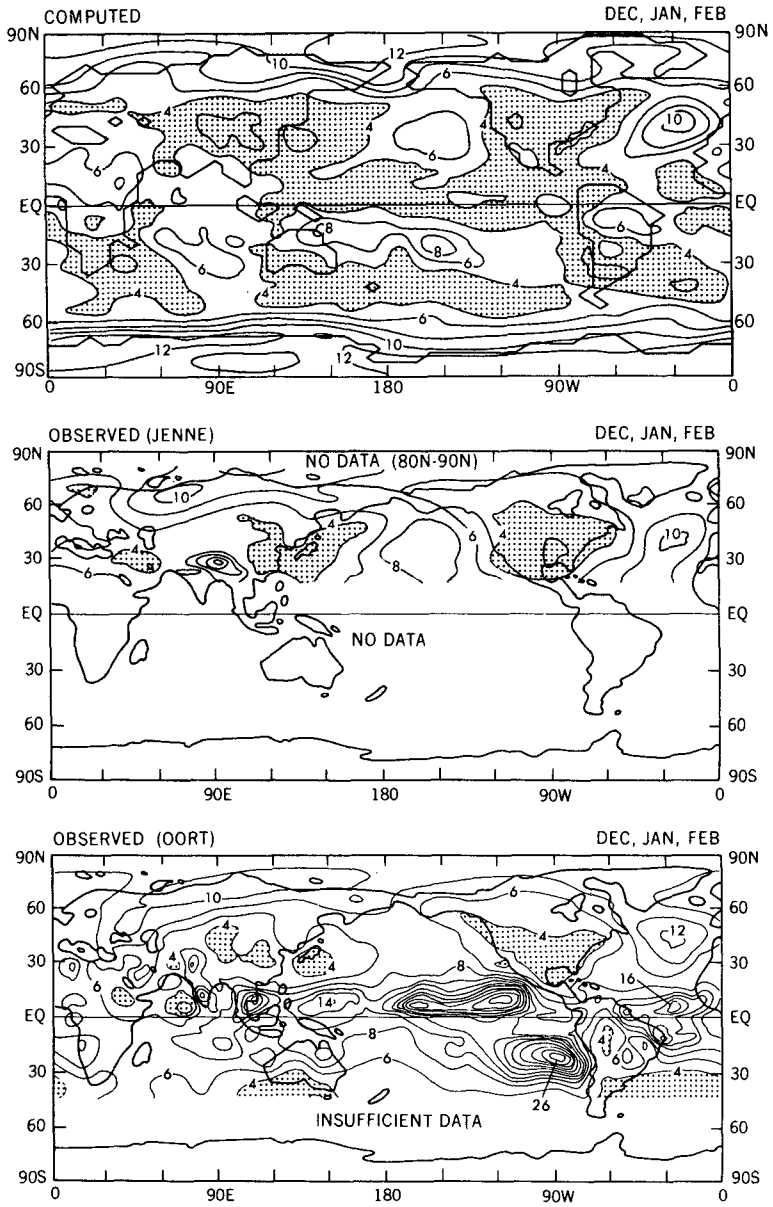

FIG. 5.13. Geographical distributions of decay time scale (τ_0, days) of 1000 mb geopotential height computed from Eq. (5) for the Dec–Jan–Feb season. Top: simulated. Middle: observed, Jenne. Bottom: observed, Oort.

from the variability of daily and monthly mean 1000 mb geopotential height for Dec–Jan–Feb season is shown in Fig. 5.13. Also included in Fig. 5.13 are two observed distributions. One is based on data from the last 15 years in the observational record compiled by Jenne. The other is based on the 10-year data set of Oort. Fig. 5.14 contains corresponding distributions for the Jun–July–Aug season. In both seasons, large values of τ_0 are found near the poles of the model. While the general level of model persistence (as indicated by τ_0) is in broad agreement with observations in high latitudes of the Northern Hemisphere, the distribution of τ_0 is not in agreement with observations near the North Pole. In both seasons, the polar maximum of the model is located north of the Bering Strait, while observed maxima are located near Greenland in the Jun–Jul–Aug season, and along the northern coast of Eurasia in the Dec–Jan–Feb season.

In the Dec–Jan–Feb season in middle latitudes of the Northern Hemisphere, τ_0-maxima in the model atmosphere are located over mid-oceanic regions and minima are located over North America and an area extending from eastern Asia into the western Pacific. These locations of maxima and minima are consistent with the discussion of Madden (1976) who suggested that maximum values of τ_0 tend to be located in regions where frequent blocking is expected

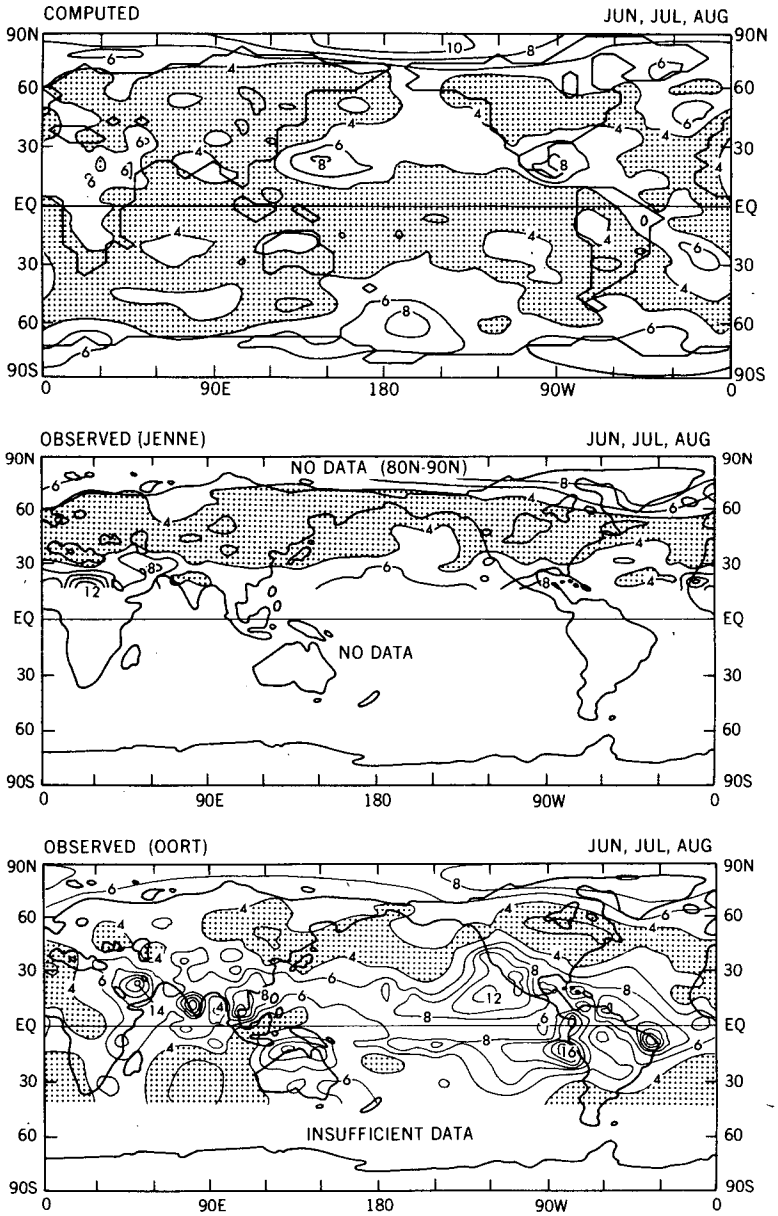

FIG. 5.14. As in Fig. 5.13 except for the Jun–Jul–Aug season.

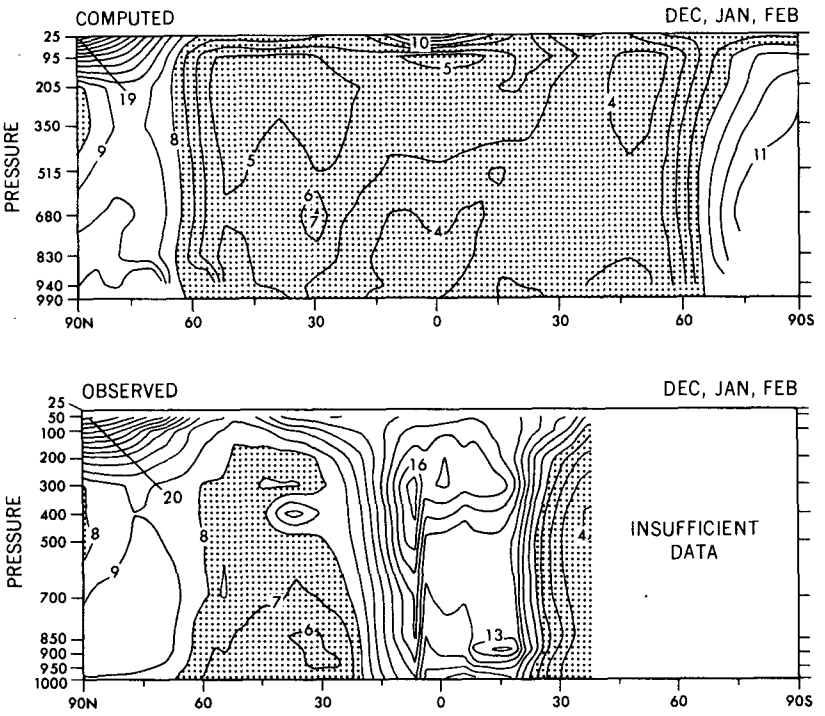

FIG. 5.15. Latitude–pressure distributions of zonal mean decay time scale (τ_0, days) of 1000 mb geopotential height computed from Eq. (5) for the Dec–Jan–Feb season. Top: simulated. Bottom: observed, Oort.

and minimum values tend to be located in regions where cyclogenesis is expected. For the model in the Jun–Jul–Aug season, similar features also are evident in middle latitudes of the Northern Hemisphere, though they are less distinct than in winter. Many of the characteristics of the model distributions described above are indicated in the observed distributions in both seasons.

In both seasons, the persistence of 1000 mb geopotential height over the model tropics is much lower than the observed. This discrepancy is particularly large over the eastern Pacific[3] and is indicative of the absence of long-term fluctuations such as the Southern Oscillation in the model atmosphere. Incorporation of the ocean–atmosphere interaction into the model appears to be necessary for the successful simulation of surface pressure variability in the tropics. The failure of the model in simulating the Southern Oscillation is evident in the results of the companion study of Lau (1981).

Latitude–pressure profiles of the zonal mean decay time scale of the model are compared with observational distributions as derived from the record compiled by Oort in Fig. 5.15 for the Dec–Jan–Feb season, and in Fig. 5.16 for the Jun–Jul–Aug season. Such profiles are zonal averages of τ_0 calculated from daily and monthly mean 1000 mb geopotential heights. In general, the decay time scale of the model is relatively large in the stratosphere of the winter hemisphere, particularly in high latitudes. In the model troposphere, it is large in the polar regions during both summer and winter seasons. Most of these characteristics are evident in the profile of zonal mean decay time scale of the actual atmosphere.

In general the decay time scale in middle latitudes of the model is much less than in polar regions. From winter to summer, this region of minimum persistence extends poleward. Qualitatively, a similar feature is evident in the observed distributions except that the persistence of the model is slightly less than observed at nearly all tropospheric levels in middle and high latitudes.

In tropical regions, from 20°N to 20°S, decay time scales obtained from model results are much shorter than those obtained from observations. For the Dec–Jan–Feb season, the difference is large at all levels, while in the Jun–Jul–Aug season, the difference is somewhat smaller near the earth's surface.

The largest difference between computed and observed decay time scales of 1000 mb geopotential height in the tropics previously was shown to occur in the eastern Pacific where large sea surface

[3] The magnitude of the very large values of τ_0 observed in the eastern Pacific is not certain since Eq. (5) holds only when $\tau_0 \ll T$.

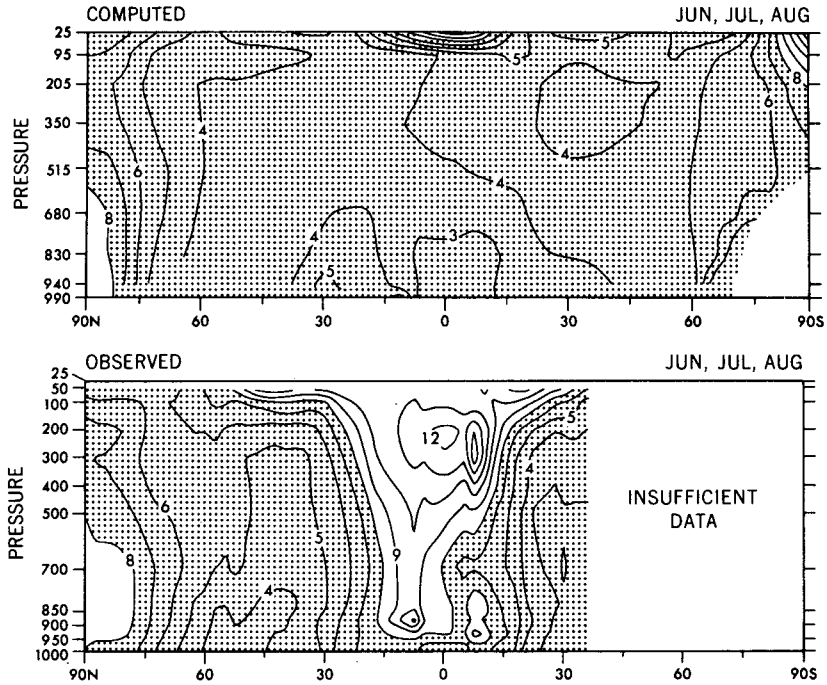

FIG. 5.16. As in Fig. 5.15 except for the Jun–Jul–Aug season.

temperature anomalies associated with El Niño are known to occur. Such variations excite long-term fluctuations in the large-scale pressure patterns in the tropics. In addition, it has been noted (from unpublished results) that the model fails to simulate the quasi-biennial oscillation observed in the upper troposphere and lower stratosphere of the tropics. This model failure is, no doubt, also reflected in the large differences between computed and observed zonal mean decay time scale in the upper troposphere of the tropics.

6. Variability of temperature

a. Geographical distributions

Geographical distributions of the annually averaged standard deviation of daily, monthly and annual mean surface air temperature of the model are illustrated in Fig. 6.1. In all three distributions, standard deviations are much larger over continents than over oceans with prescribed surface temperature. They are at a maximum over the high-latitude portions of the North American and Eurasian continents and are at a minimum over equatorial oceanic regions. In general, the distributions of daily, monthly and yearly standard deviations resemble one another. This similarity suggests the possibility that a daily record of surface air temperature resembles a red noise time series as was the case with surface pressure.

Fig. 6.2 contains an observational counterpart of the variability distribution of annual mean surface air temperature of the model shown in Fig. 6.1. This figure indicates that the land–sea contrast in the magnitude of variability is also evident in the observed distribution of standard deviation of annual mean surface air temperature. Furthermore, zones of relatively large variability in high-latitude regions of the model continents also appear in the observed distribution. Although the model tends to underestimate the magnitude of annual variability over tropical oceans, it succeeds in reproducing the general characteristics of the geographical distribution of standard deviation of annual mean surface air temperature of the atmosphere.

b. Zonal means

To examine the vertical distribution of temperature variability, Figs. 6.3 and 6.4 are contructed. In these figures, the latitude–pressure distributions of the annual, zonal mean standard deviation of the daily and monthly mean temperature of the model atmosphere are compared with corresponding distributions for the actual atmosphere obtained from the data of Oort. For the model atmosphere, variability of both daily and monthly mean temperature is at a minimum in the equatorial troposphere. In addition, it appears significant that in high latitudes of the model, the standard deviation of both daily

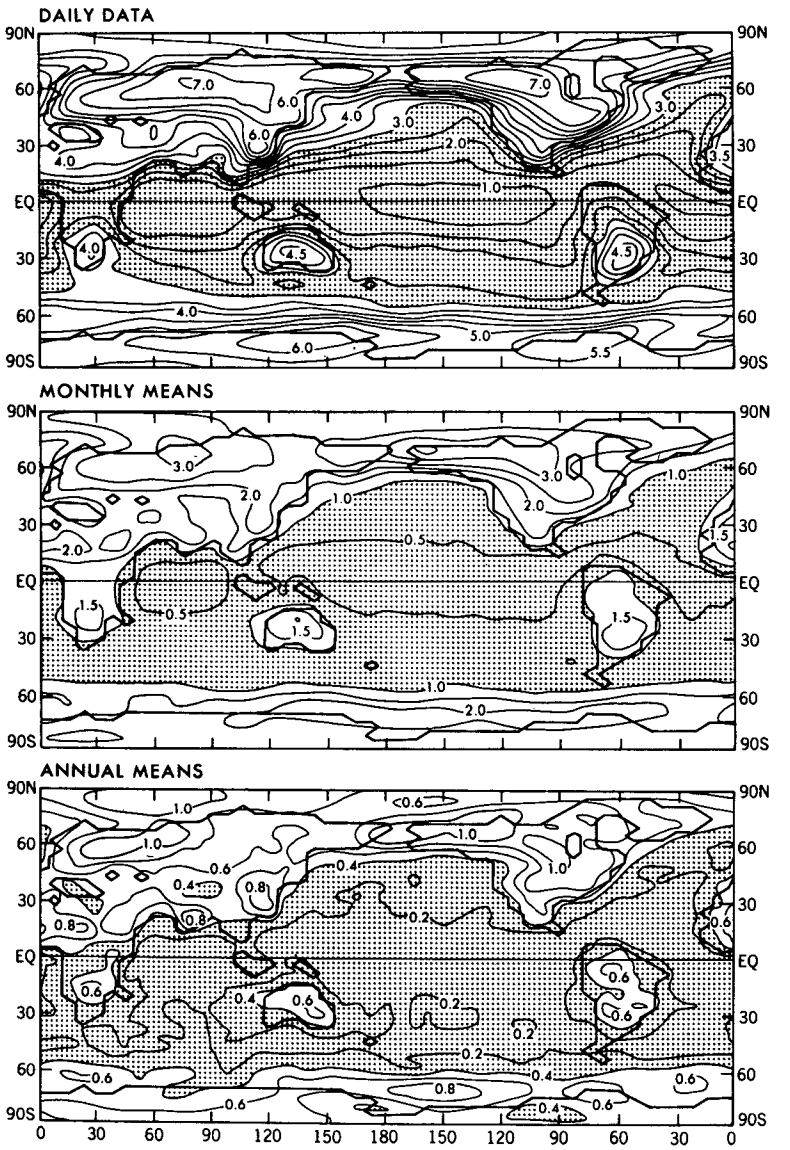

FIG. 6.1. Annual mean standard deviation of daily (top), monthly mean (middle), and annual mean (bottom) surface air temperature (K) of the model. For the top two distributions, annual mean standard deviation is computed as the square root of the arithmetic mean of variances for the 12 months.

and monthly mean temperature is relatively small near the tropopause level where the meridional temperature gradient is very small, and is large near the earth's surface where the meridional temperature gradient is at a maximum. Similar characteristics are evident in the observed distributions.

There are, however, differences between the observed and computed distributions. In the middle troposphere of high latitudes, simulated standard deviations of both daily and monthly mean temperature are smaller than the corresponding values for the actual atmosphere. This result is related to the model's underestimation of the geopotential height variability described in the preceding section. In the upper troposphere and lower stratosphere of the tropics, the simulated variability of daily temperature fluctuations is slightly larger than the corresponding observed variability, whereas the reverse is the case with respect to the variability of monthly mean temperatures. This implies that temperature fluctuations in the model atmosphere have shorter time scales than those of the actual atmosphere, as discussed in the following subsection.

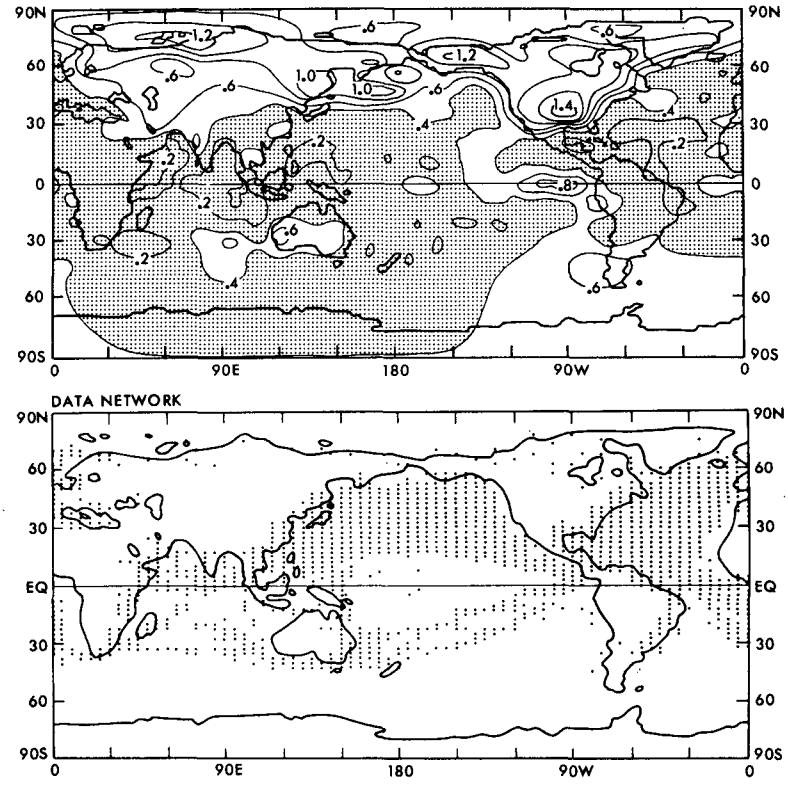

FIG. 6.2. Standard deviation of observed annual mean surface air temperature (K), Oort (personal communication). Bottom half displays the distribution of the observational data used to create the top half of this figure.

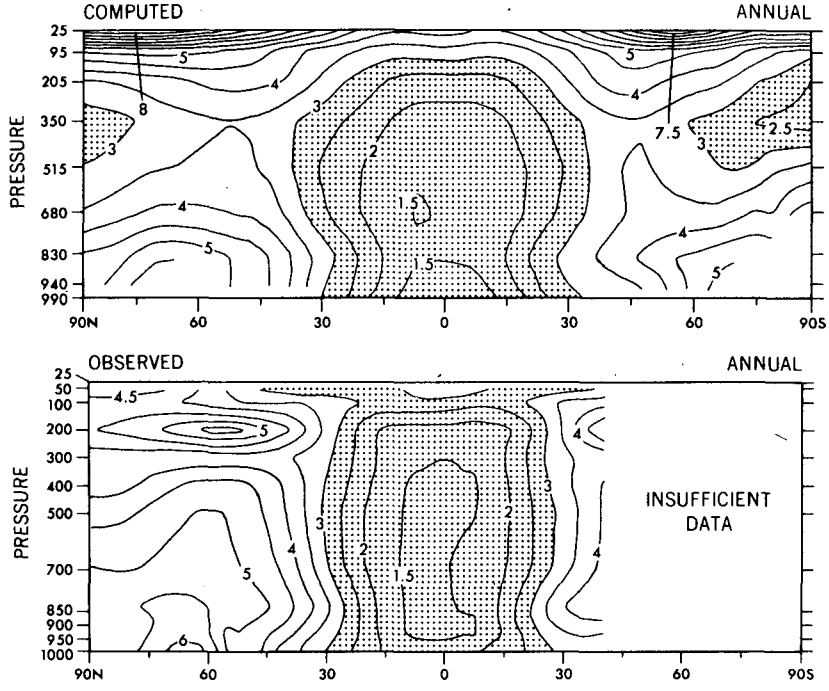

FIG. 6.3. Latitude–pressure distributions of zonally averaged standard deviation of daily temperature (K). Top: simulated. Bottom: observed, Oort. Distributions are averaged over the annual cycle as in Fig. 6.1.

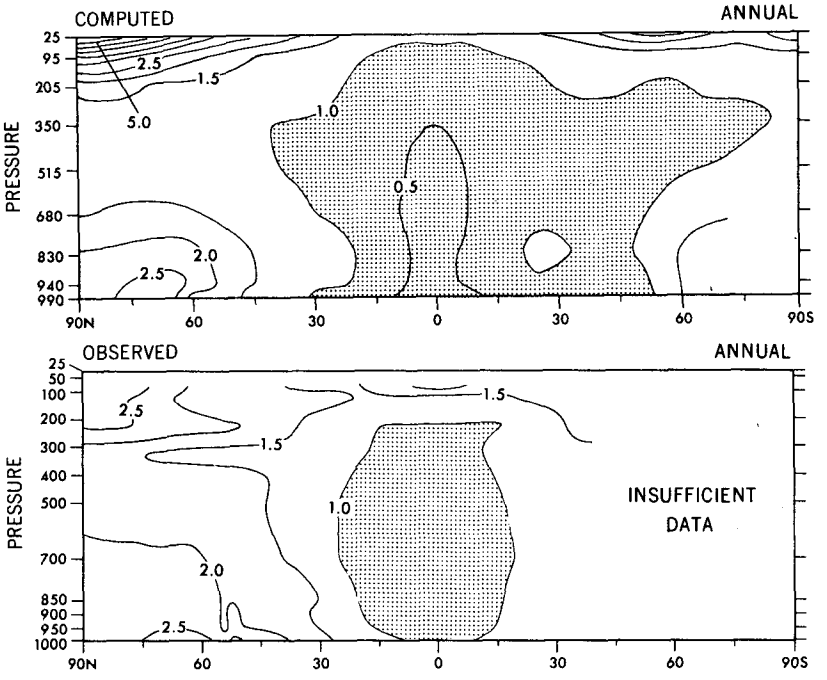

FIG. 6.4. As in Fig. 6.3 except for monthly mean temperature.

c. Persistence

To compare the persistence of temperature fluctuations in the model atmosphere with that of actual atmosphere, Fig. 6.5 is constructed. This figure illustrates the latitude–pressure distributions of zonal and annually averaged decay time scale τ_0 computed from standard deviations of daily and

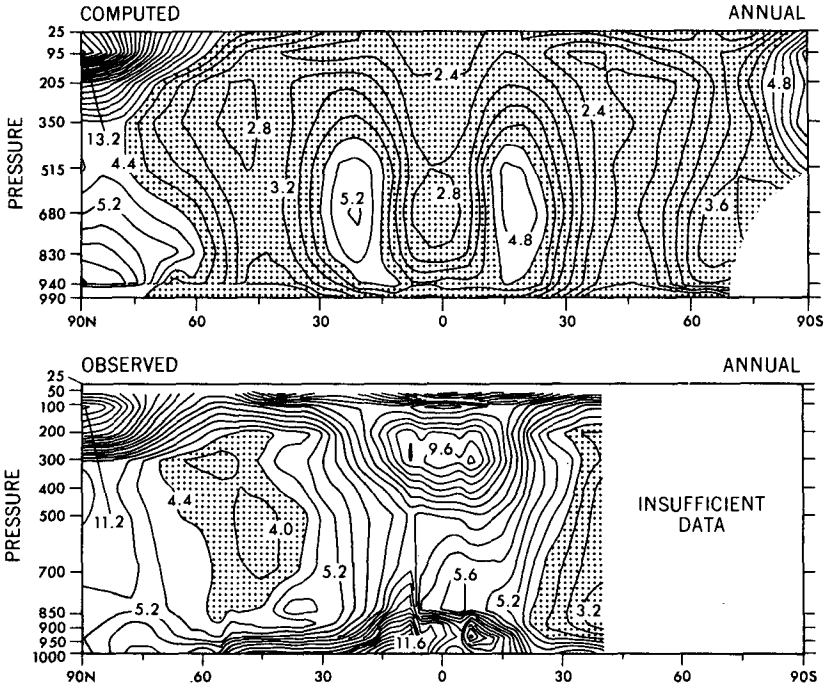

FIG. 6.5. Latitude–pressure distribution of zonally averaged decay time scale (τ_0, days) of surface air temperature as computed from Eq. (5). Top: simulated. Bottom: observed, Oort. Distributions are calculated using data averaged over the annual cycle as in Fig. 6.1.

monthly mean temperature for both the model and the actual atmosphere. In general, the zonal mean decay time scale of the model is significantly smaller than the corresponding time scale from the actual atmosphere. One may note, however, some qualitative similarities between the simulated and observed distributions. For example, in the model troposphere τ_0 is at a minimum in middle latitudes and increases equatorward and poleward, in qualitative agreement with the observed distribution. Similar characteristics are noted in the simulated distributions of zonal mean decay time scale for geopotential height described in Section 5. One of the most notable differences between the observed and computed distributions is again evident in tropical regions. According to Fig. 6.5, the zonal mean decay time scale is particularly large in the upper tropical troposphere, where it is very small in the model atmosphere. A similar discrepancy is evident with respect to the persistence fields of geopotential height shown in Figs. 5.15 and 5.16.

7. Fluctuations of zonal and hemispheric mean temperature

In previous sections, the local variability of key variables of the model is compared with that of the actual atmosphere. In this section, the temporal fluctuations of the departure of hemispheric mean surface air temperature from the normal (15-year mean) seasonal climatology is examined. This is of great interest because hemispheric mean temperature is often used as a key indicator of long-term climate variations.

Fig. 7.1 contains a latitude–time distribution of zonal mean surface air temperature departure smoothed by a 12-month running mean operator. In both hemispheres the fluctuations of zonal mean surface air temperature are particularly large in high latitudes, and very small near the equator. These results are consistent with the features of Figs. 6.1 and 6.2 which also show that the local variability of annual mean surface air temperature increases with increasing latitude.

Fig. 7.1 also shows evidence of very long-term fluctuations in the model's surface air temperature. For example, positive surface air temperature anomalies exist near the north pole in year 2 of the model integration. During the next four model years, this feature apparently shifts equatorward. A similar shift apparently takes place from years 7 to 15. The interannual variation of hemispheric mean surface air temperature may simply be a red noise manifestation of daily weather fluctuations with a relatively short decay time scale of 4–5 days. However, these variations are notable enough to warrant further study.

Monthly means of surface air temperature averaged over the entire Northern Hemisphere are shown in Fig. 7.2 for both the 15-year record of the model integration and the 25-year record of observational results compiled by Yamamoto *et al.*

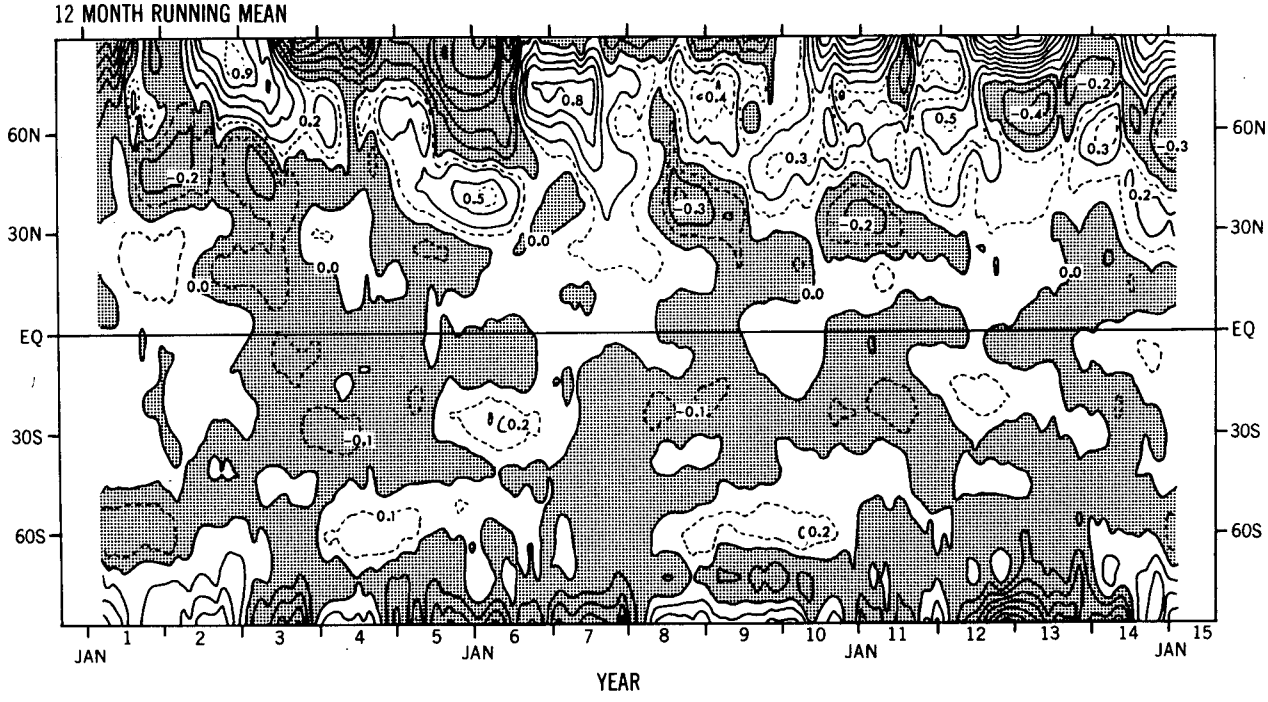

FIG. 7.1. Latitude–time distribution of 12-month running mean of zonally, monthly averaged surface air temperature departure (from the 15-year mean of each month, K).

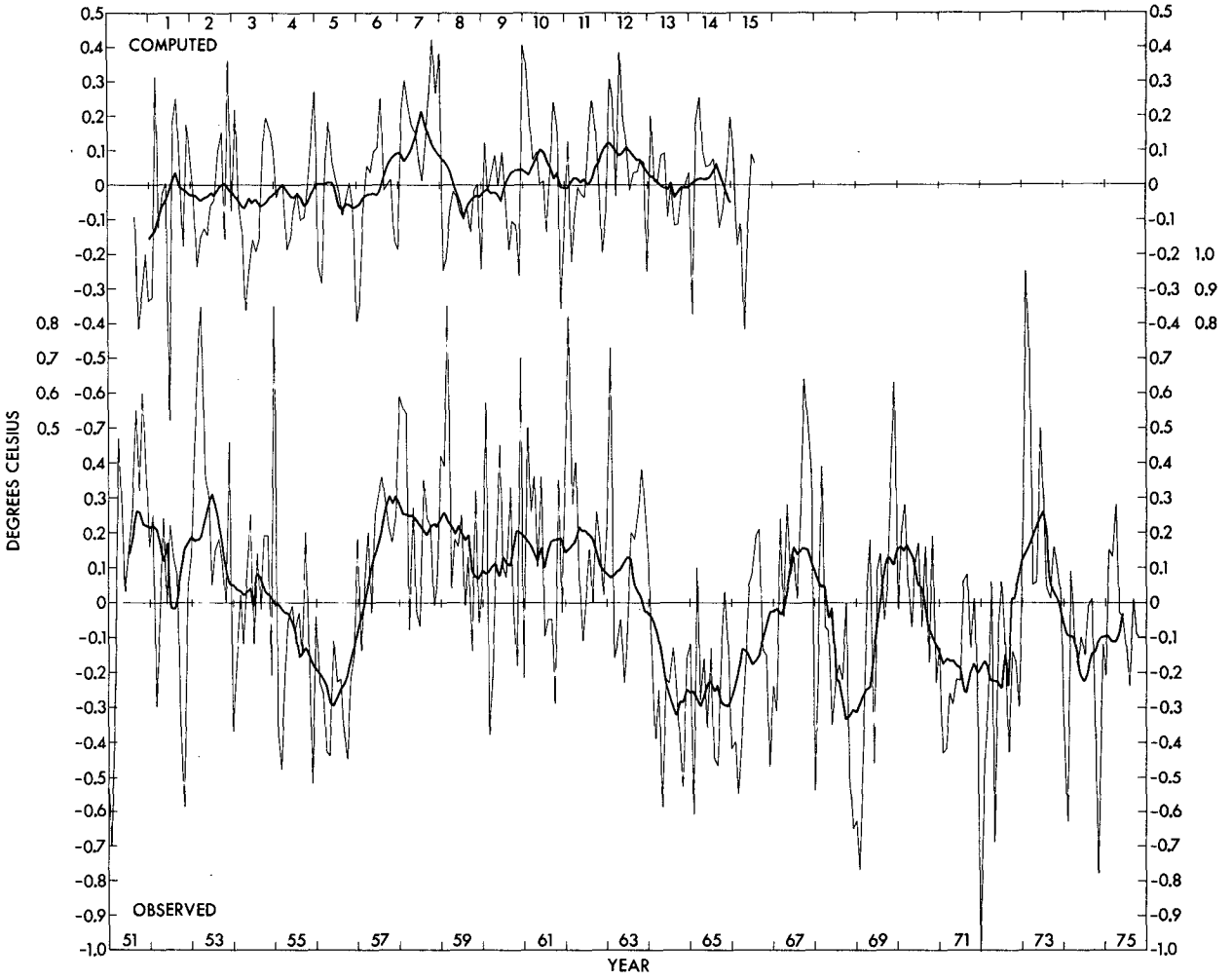

FIG. 7.2. Temporal variations of monthly, Northern Hemispheric mean surface air temperature departure (from the 15-year mean for each month, K). Thin line curves indicate monthly data; heavy line curves represent 12-month running means of the monthly data. Top: simulated. Bottom: observed, Yamamoto (1975).

(1975). In both cases, the annual cycle is removed from the time series. To emphasize characteristics of fluctuations which have time scales that are much longer than one month, 12-month running means of the above time series also are added to the figure. Visual comparison of the time series of monthly means reveals that both observed and simulated time series contain large episodic increases and decreases. In such episodes, values of this quantity increase or decrease up to 1.0°C in a relatively short period of one or two months. It is important to note that the amplitude of the observed fluctuations is significantly larger than for model fluctuations. This difference is particularly evident in the comparison of the 12-month running means. For example, from 1951 to 1956 and from 1958 to 1965, large downward trends of 12-month running mean surface air temperature extend over many years in the observed record, a feature not as apparent in the model results.

TABLE 1. Standard deviation of Northern Hemisphere mean surface air temperature (°C).

	Observed data	
	Yamamoto *et al.* (1975)	Model data
Monthly means	0.29	0.16
3-Monthly running means	0.22	0.11
12-Monthly running means	0.16	0.05

The difference between the observed and simulated variability is quantified in Table 1 which contains the standard deviations of monthly, 3 and 12 monthly running mean values of surface air temperature of both the model and the actual atmosphere. According to this table, the standard deviation of monthly, hemispheric mean surface air

temperature of the model atmosphere amounts to ~55% of the corresponding standard deviation for the actual atmosphere. For the three monthly running means, the model variability is 50% of the observed value, and for 12-month running means, it is only 31%. In short, results contained in Table 1 indicate that the standard deviations of hemispheric mean surface air temperature of the model atmosphere are significantly smaller than the corresponding standard deviations of the actual atmosphere. The discrepancy becomes larger with increasing averaging period.

It is important, however, to recognize that the observed variability of hemispheric mean temperature may not be accurate. This possibility is underscored by the fact that observed variability of annual mean surface air temperature as compiled by Yamamoto *et al.* (1975) is approximately twice as large as that of Yamamoto and Hoshiai (1979). The variability of the latter is very similar to that of the model while the variability of the former is substantially larger than that of the model. The variability as determined by Angell and Korshover (1977) appears to be very similar to that of Yamamoto *et al.* (1975). In addition, extended comparisons by Angell and Korshover (1977) indicate that their results are similar to those of Reitan (1974) and Budyko (1969, 1977), although the latter two results appear to contain a slightly lower level of variability.

It is difficult to understand the reasons for the large differences between the level of observed variability in the results of Yamamoto and Hoshiai (1979) and the corresponding magnitudes in the studies of Yamamoto *et al.* (1975), Angell and Korshover (1977), Reitan (1974) and Budyko (1969, 1977). However, Barnett (1978) and Yamamoto and Hoshiai (1980) point out that the nonuniformity of the network of observing stations chosen for the analysis may result in a large error in the estimation of hemispheric mean temperature. In the network chosen by Angell and Korshover (1977, Fig. 1), the density of observational stations over oceans is much less than over continents in the Northern Hemisphere. Since they assumed equal weight for both oceanic and continental data, continental temperature fluctuations have a disproportionately large influence on the variability of hemispheric mean temperature. As described in the preceding section, the standard deviation of local temperature fluctuations tends to be generally larger over continental regions than over oceanic regions. Therefore, their network may yield an overestimated standard deviation of hemispheric mean temperature. Qualitatively similar overestimation may result from the usage of the cubic spline interpolation technique adopted by Yamamoto *et al.* (1975) when the density of the observational network varies from continents to oceans. On the other hand, Gandin's optimum interpolation technique (Gandin, 1963, 1969) as modified and used by Yamamoto and Hoshiai (1979) tends to underestimate the contribution from data-sparse (oceanic) regions. In the computation of hemispheric mean temperature deviation, Yamamoto and Hoshiai assumed that the temperature deviation is equal to zero at grid points which have no observational data within the range of the characteristic scale of horizontal temperature variations. This assumption is partially responsible for the underestimation mentioned above.

In order to lend greater understanding by way of example, standard deviations of time mean, Northern Hemisphere mean surface air temperature of the model are recomputed using model data only at the Angell-Korshover network rather than using the complete array of model data. The standard deviations thus computed are approximately twice as large as the original values obtained from the data at every grid point. For example, the value of standard deviation increases from 0.16 to 0.31 for monthly data, from 0.11 to 0.20 for three-monthly data, and from 0.05 to 0.11 for annual mean temperature data. These results do not necessarily imply that the Angel-Korshover network yields a similar overestimation when it is used for the analysis of the observed surface air temperature. However, the present analysis suggests that the discrepancy between observed and simulated results may not be as large as Table 1 indicates. Considering this observational uncertainty, the standard deviation of annual, hemispheric mean surface air temperature of the model potentially amounts to a substantial fraction of the corresponding standard deviation for the actual atmosphere. It is important to note that the present model does not include various processes with long time constants, such as secular variation of atmospheric turbidity and ocean–atmosphere interaction. The results of this section suggest that one cannot disregard the effect of nonlinear dynamical processes in the atmosphere when one discusses the interannual variation of surface air temperature.

8. Summary and conclusions

The spectral atmospheric circulation model described here simulates not only the distribution of surface pressure, but also that of its variability. Except in tropical regions, the model is successful in simulating the distribution of local variability of daily and monthly means. Even for annual means, a high percentage of observed variability is realized by the model despite an absence of interannual variability of underlying oceanic temperatures. In general, the model's ability to simulate the variability of geopotential height deteriorates with increasing altitude.

The model also possesses skill in simulating the geographical distribution of the local variability of surface air temperature in the atmosphere. For example, the variability of surface air temperature over continents is much larger than the variability over oceans. It is particularly large over the high-latitude portions of continents, in agreement with observed characteristics.

In qualitative agreement with the characteristic of the actual atmosphere (Leith, 1973; Madden, 1976), global mean values of standard deviation of daily, weekly, monthly and yearly mean surface pressure may be fitted approximately by a corresponding set of standard deviations of a red noise time series with a decay time scale of 4–5 days. However, it appears that the temporal variation of surface pressure also includes minor contributions from disturbances with much longer decay time scales. The structures of the disturbances with relatively long decay time scales are the subject of an extensive analysis in a companion paper by Lau (1981).

In general, the persistence of the local fluctuations of simulated surface pressure as indicated by a single correlation decay time scale, τ_0, is significantly shorter than the corresponding persistence for the actual atmosphere. This discrepancy partly results from a tendency of this low-resolution spectral model to accumulate kinetic energy near the short end of energy spectrum (Manabe *et al.*, 1979). It is encouraging, however, that the model simulates some of the characteristics of the horizontal distribution of decay time scale for the surface pressure fluctuations. For example, the winter distribution of τ_0 for the model indicates relatively large persistence of surface pressure over the north Pacific and North Atlantic where blocking in the pressure patterns frequently occurs in the actual atmosphere. In general, the simulated decay time scale is relatively short in middle latitudes, where development of cyclones predominates, and increases poleward in agreement with observed characteristics. However, the model fails to simulate the large persistence of the pressure field observed in the entire tropical troposphere. The discrepancy between computed and observed persistence is particularly large over the eastern equatorial Pacific where long-term fluctuations of sea surface temperature associated with the southern oscillation predominate.

It is shown that the model has a relatively poor performance in simulating the variability of temperature and geopotential height in the tropics. This result appears to be consistent with the recent study of Charney and Shukla (1981). By use of results from several relatively short time integrations of a general circulation model developed at the Goddard Laboratory for Atmospheric Sciences (NASA), they suggest that fluctuations in the atmospheric circulation occurring in the absence of boundary anomalies account for most of the variability of monthly mean rate of precipitation and monthly mean sea level pressure in the middle latitudes but not in the tropics. According to their speculation, the missing element of the model tropics is probably some boundary forcing (e.g., anomalies of sea surface temperature and surface albedo). It is probable that the absence of the interaction between the atmosphere and ocean also explains the failure of the present model in simulating the relatively large persistence in the fields of pressure and temperature in the tropics.

In view of the increased interest in long-term fluctuations of hemispheric (or global) mean temperature, the variability of hemispheric mean surface air temperature is also examined in this study. A clearcut evaluation of the model's performance in this regard is somewhat hampered by observational uncertainty. However, the standard deviation of annually averaged, Northern Hemisphere mean surface air temperature of the model may account for a substantial fraction of the corresponding standard deviation for the actual atmosphere. This result suggests that one cannot completely disregard the contributions from nonlinear dynamical interaction processes in the atmosphere when one discusses the interannual variation of hemispheric mean temperature.

The results described here are obtained from a general circulation model with low computational resolution. When more computer resources become available, it is desirable to repeat the present numerical experiment by use of a model with higher computational resolution which is capable of reproducing the spectral distribution of kinetic energy of the atmospheric motion with better fidelity. Nevertheless, the results from the present study encourage its authors to use a similar model for performing preliminary numerical experiments designed for the identification of processes responsible for causing climate fluctuations.

Acknowledgments. The authors are very much indebted to A. Oort for providing us with summary tapes used for his observational variability analyses. Because of this major contribution, it was possible to carry out an extensive comparison between the observed and simulated variability. J. Angell and R. Yamamoto kindly provided the authors with the data of hemispheric mean surface air temperature and gave them valuable comments on the reliability of these data. The constructive comments of Y. Hayashi, I. Held, N. Lau, A. Oort and M. Stefanick were very useful for improving the manuscript. L. Dimmick participated in the analysis of the results by constructing and running the computer programs for the data processing. D. Daniel effec-

tively managed the numerical time integration of the model. The authors wish to acknowledge J. Kennedy for typing and P. Tunison and his staff for their excellent drafting support. Particularly, it is a pleasure to thank J. Smagorinsky, who has given wholehearted support throughout the course of this study.

REFERENCES

Angell, J., and J. Korshover, 1977: Estimates of the global change in tropospheric temperature between 1958 and 1973. *Mon. Wea. Rev.*, **103**, 1007–1012.

Barnett, T. P., 1978: Estimating variability of surface air temperature. *Mon. Wea. Rev.*, **106**, 1353–1367.

Blackmon, M. L., and N.-C. Lau, 1980: Regional characteristics of the Northern Hemisphere wintertime circulation: A comparison of the simulation of the GFDL general circulation model with observation. *J. Atmos. Sci.*, **37**, 497–514.

Bourke, W., 1974: A multi-level model. I. Formulation and hemispheric integrations. *Mon. Wea. Rev.*, **102**, 688–701.

Budyko, M. I., 1969: The effect of solar radiation variation on the climate of the earth. *Tellus*, **21**, 611–619.

——, 1977: On present-day climatic changes. *Tellus*, **29**, 193–204.

Charney, J., and J. Shukla, 1981: Predictability of monsoons. *Monsoon Dynamics*, Sir James Lighthill and R. P. Pearce, Eds., Cambridge University Press, 99–110.

Chervin, R. M., 1980: Estimates of first- and second-moment climate statistics in GCM simulated climate ensembles. *J. Atmos. Sci.*, **37**, 1889–1902.

Crutcher, H. L., and J. M. Meserve, 1970: Selected level heights, temperatures and dew points for the Northern Hemisphere. NAVAIR 50-1C-52. U.S. Govt. Printing Office, Washington, DC.

Gandin, L. S., 1963: *Objective Analysis of Meteorological Fields*. Israel Program for Scientific Translation, Jerusalem, 242 pp.

——, 1969: Objective analysis. *Lectures on Numerical Short-Range Weather Prediction*. WMO, Hydrometeoizdat, Leningrad, 657–700.

Gordon, C. T., and W. Stern, 1974: Spectral modelling at GFDL. The GARP Programme on numerical experimentation. Report of the International Symposium on Spectral Methods in Numerical Weather Prediction, Copenhagen, WMO Rep. No. 7, 46–80.

Hahn, D. G., and S. Manabe, 1979: Simulation of atmospheric variability. *Proceedings of the Fourth Annual Climate Diagnostics Workshop*, NOAA, University of Wisconsin, Madison, 398–402. [NTIS PB80201130].

Holloway, J. L., Jr., and S. Manabe, 1971: Simulation of climate by a global general circulation model: I. Hydrologic cycle and heat balance. *Mon. Wea. Rev.*, **99**, 335–370.

Jenne, R. L., 1975: Data sets for meteorological research. NCAR Tech. Note TN/IA-111, National Center for Atmospheric Research, 172 pp. [NTIS PB246564].

Lacis, A. A., and J. E. Hansen, 1974: A parameterization for the absorption of solar radiation in the earth's atmosphere. *J. Atmos. Sci.*, **31**, 118–133.

Lau, N. C., 1981: A diagnostic study of recurrent meteorological anomalies appearing in a 15-year simulation with a GFDL general circulation model. *Mon. Wea. Rev.*, **109**, 2287–2311.

Leith, C. E., 1973: The standard error of time-average estimates of climatic means. *J. Appl. Meteor.*, **12**, 1066–1069.

Madden, R. A., 1976: Estimates of the natural variability of time-averaged sea-level pressure. *Mon. Wea. Rev.*, **104**, 942–952.

Manabe, S., 1969: Climate and ocean circulation, Part I, The atmospheric circulation and hydrology of the earth's surface. *Mon. Wea. Rev.*, **97**, 739–774.

——, D. G. Hahn and J. L. Holloway, Jr., 1979: Climate simulations with GFDL spectral models of the atmosphere: Effect of spectral truncation. Rep. of the JOC Study Conference on Climate Models: Performance, Intercomparison and Sensitivity Studies, Washington DC, 3–7 April 1978. *GARP Publ. Ser.* No. 22, Vol. 1, 41–94. [NTIS N8027917].

——, J. Smagorinsky and R. F. Strickler, 1965: Simulated climatology of a general circulation model with a hydrologic cycle. *Mon. Wea. Rev.*, **93**, 769–798.

Oceanographic Office, U.S. Navy, 1969: Monthly charts of mean, minimum and maximum sea surface temperature of the North Pacific Ocean. SP-123, Washington, DC. [Available from Defense Mapping Agency Depot, 5801 Tabor Ave., Philadelphia, PA 19120.]

——, 1967a: Monthly charts of mean, minimum, and maximum sea surface temperature of the Indian Ocean. SP-99, Washington, DC. [Available from Defense Mapping Agency Depot, 2801 Tabor Ave., Philadelphia, PA 19120.]

——, 1967b: *Oceanographic Atlas of the North Atlantic Ocean, Section II: Physical Properties*. Publ. No. 700, Washington, DC. [Available from Defense Mapping Agency Depot, 2801 Tabor Ave., Philadelphia, PA 19120.]

——, 1958: *Oceanographic Atlas of the Polar Seas, Part II: Arctic*. H.O. Publ. No. 705, Washington, DC. [Available from Defense Mapping Agency Depot, 2801 Tabor Ave., Philadelphia, PA 19120.]

——, 1957: *Oceanographic Atlas of the Polar Seas, Part I. Antarctic*. H.O. Publ. No. 705, Washington, DC. [Available from Defense Mapping Agency Depot, 5801 Tabor Ave., Philadelphia, PA 19120.]

——, (U.S. Navy Hydrographic Office), 1944: *World Atlas of Sea Surface Temperatures*, 2nd ed. H.O. Publ. No. 225, Washington, DC. [Available from Defense Mapping Agency Depot, 5801 Tabor Ave., Philadelphia, PA 19120.]

Oort, A. H., 1978: Adequacy of the rawinsonde network for global circulation studies tested through numerical model output. *Mon. Wea. Rev.*, **106**, 174–195.

——, 1982: *Global Atmospheric Circulation Statistics, 1958–1973*. NOAA Prof. Paper, U.S. Government Printing Office, Washington, DC (in press).

Reitan, C. H., 1974: A climate model of solar radiation and temperature change. *Quarternary Res.*, **4**, 25–38.

Rodgers, C. D., and D. C. Walshaw, 1966: The computation of infra-red cooling rate in planetary atmospheres. *Quart J. Roy. Meteor. Soc.*, **92**, 67–92.

Stefanick, M., 1981: Space and time scales of atmospheric variability. *J. Atmos. Sci.*, **38**, 988–1002.

Stone, H. M., and S. Manabe, 1968: Comparison among various numerical models designed for computing infrared cooling. *Mon. Wea. Rev.*, **96**, 735–741.

Taljaard, J. J., H. van Loon, H. L. Crutcher and R. L. Jenne, 1969: *Climate of the Upper Air. Part I. Southern Hemisphere, Vol. 1, Temperatures, dew points and heights at selected pressure levels*. NAVAIR, 50-1C-55, unpaginated. [Available from Naval Weather Service, Command, Washington Naval Yard, Building 200, Washington, DC. 20390.]

van Loon, H., 1967: A climatological study of the atmospheric circulation in the Southern Hemisphere during the IGY: Part II. *J. Appl. Meteor.*, **6**, 803–815.

——, and R. L. Jenne, 1974: Standard deviations of monthly mean 500 and 100-mb heights in the Southern Hemisphere. *J. Geophys. Res.*, **79**, 5661–5664.

Yamamoto, R., T. Iwashima and M. Hoshiai, 1975: Change of the surface air temperature averaged over the Northern Hemisphere and large volcanic eruptions during the years 1951–1972. *J. Meteor. Soc. Japan*, **53**, 482–485.

——, and M. Hoshiai, 1979: Recent change of the Northern Hemisphere mean surface air temperature estimated by optimum interpolation. *Mon. Wea. Rev.*, **107**, 1239–1244.

——, and ——, 1980: Fluctuation of Northern Hemisphere mean surface air temperature during recent 100 years, estimated by optimum interpolation. *J. Meteor. Soc. Japan*, **58**, 187–193.